Chapter 3

Measuring of Homonuclear Dipole-Dipole couplings

In this chapter a various NMR r.f. pulse techniques will be used and compared for measuring dipole-dipole couplings in amorphous polymers. If chemical shift anisotropies (CSA) can be neglected with comparison to the dipolar coupling strength as well as B_1 field inhomogeneities the simple r.f. pulse experiment under MAS can be used for estimating dipolar couplings. Already existing theoretical analysis valid for fast spinning regime ([Got96, Gra97a]) are extended for moderate spinning speeds in section 3.1. As an experimental example hexamethylbenzene (HMB) has been chosen for evaluating the dipolar coupling. In sections 3.2 and 3.3 high resolution multiple-pulse sequences like C7, POST C7, BABA and DRAMA which are suitable for site selective measuring of the dipolar couplings under fast MAS are compared. Their efficiencies are studied with connection to elastomers. Initial part of the build-up curves is used to evaluate the relative residual dipolar couplings in more complicated systems like natural rubber in section 3.3.2. In section 3.4 the high resolution MAS spin counting experiment is presented. POST C7 pulse sequence (see section 2.5.1.3) has been used to measure the sizes of the dipolar spin clusters in adamantane. It is shown that POST C7 provides comparable results to the already existing measurements performed by Geen et al. ([Gee99]) with C7 pulse sequence. In the last section (section 3.5) double quantum (DQ) as well as multiple quantum (MQ) coherences on static solids are presented. DQ filtering techniques (see section 4.3) are applied for eight pulse sequence and for thirty-two pulse sequence, respectively. Both pulse sequences can be used for measuring relative dipolar couplings. Their efficiencies with

respect to elastomers are compared in section 3.5.1. In section 3.5.2 MQ spin counting experiment on elastomers is presented. Up to the 6-th order of coherence has been measured in high crosslinked polybutadiene rubber with thirty-two pulse sequence which was up to now not reported on elastomers.

3.1 Single Quantum MAS experiment

In this section dipolar coupling will be measured from a single quantum (SQ) MAS experiment. Theoretical bases for simple one pulse MAS experiment were already done in section 1.6. Two spin-½ system coupled via dipole-dipole coupling was chosen to simulate the NMR signal (see equation (1.83)). Neglecting CSA terms it was shown that MAS generate a symmetric SQ spinning sidebands spectrum (see Figure 1.4). Comparing intensities of the spinning sidebands dipolar coupling strength d_{ij}^{II} can be calculated ([Gra97a, Fil97]). For moderate spinning speeds when $\omega_r \backsimeq d_{ij}^{II}$ an approximate solution of the equation (1.83) will be presented. It was found by our computer simulation that approximation up to the 6-th order is sufficient for this spinning regime.

For rapid spinning case ($\omega_r \gg d_{ij}^{II}$) equation (1.83) describing the signal from the dipolar coupled spin-½ pair can be formally solved. The cosine function may be expanded into the Taylor series and only up to the second-order coefficients will be considered. Calculating the powder average through angles ϑ, ψ it can be found the approximate solution

$$\tilde{S}_y^{MAS}(t) = \underbrace{1 - \frac{27}{80}\,\mu^2}_{\text{Central line}} + \underbrace{\frac{3}{10}\,\mu^2 \cos(\omega_r t)}_{\text{1. Order sidebands}} + \underbrace{\frac{3}{80}\,\mu^2 \cos(2\omega_r t)}_{\text{2. Order sidebands}} \tag{3.1}$$

with the parameter $\mu = d_{ij}^{II}/\omega_r$. Detailed derivation of the equation above can be found in Graf thesis ([Gra97a], Appendix A). Assuming the integral intensity of the first sideband I_{s1} and the integral intensity of the central line I_0 the dipolar coupling can be calculated by the help of equation (3.1) as

$$d_{ij}^{II} = \omega_r \sqrt{\frac{20\, I_{s1}/I_0}{3+\frac{27}{4}\, I_{s1}/I_0}} \quad . \tag{3.2}$$

This simple two spin system approximation can not be used if the MAS spectrum is asymmetric which can be caused by spectrometer problems or by the influence of an anisotropic coupling (e.g. B_1 field inhomogeneity, CSA). The restriction for the second order approximation can be made according to Filip et al. ([Fil97]) calculations as $\mu \leq 0.5$ ($\omega_r \geq 2d_{ij}^{II}$). This restriction can be therefore considered as a condition for very fast

spinning limit. For smaller μ the difference between the exact and the approximate result became negligible for two spin system. In general the dipolar coupling can be also calculated from the integral intensity of the second order sideband (see equation (3.1)) but for the fast spinning case ($\mu \leq 0.5$) the intensity is at least 200 times smaller than the intensity of the central line and thus due to the big experimental error of evaluating the integral it has no use.

For moderate spinning speeds the error introduced by the considering only the second-order terms increasing rapidly as μ approaches the value $\mu = 1$ (Neglecting terms of order four and higher an error of 25% is introduced to calculate ratio $\frac{\text{1.-order sideband}}{\text{central line}}$ when $\mu = 1$). The extension to higher orders is necessary to get sufficient precise results. In moderate spinning regime ($\mu \lesssim 1$) the expansion until 6-th order of equation (1.83) is sufficiently enough. Integral intensities of the central line I_0, 1.-order sideband I_{s1} and 2.-order sideband I_{s2} for powder sample were calculated and result can be written in following form

$$\begin{aligned} I_0/I_{st} &= 1 - \tfrac{27}{80}\,\mu^2 + \tfrac{2043}{35840}\,\mu^4 - \tfrac{89343}{16400384}\,\mu^6 \\ I_{s1}/I_{st} &= \tfrac{3}{20}\,\mu^2 - \tfrac{153}{4480}\,\mu^4 + \tfrac{10611}{2928640}\,\mu^6 \\ I_{s2}/I_{st} &= \tfrac{3}{160}\,\mu^2 + \tfrac{9}{2560}\,\mu^4 - \tfrac{241623}{328007680}\,\mu^6\,. \end{aligned} \tag{3.3}$$

The intensities are normalized by the integral intensity of the static NMR spectrum I_{st}. Due to the symmetry of the sideband spectrum (see e.g. Figure 1.4) only integral intensities of the one half of the spectrum are represented by symbols I_{s1} and I_{s2}. From set of equations (3.3) dipolar coupling can be directly determined similar like in equation (3.2). Three different solutions can be found comparing intensities of I_{s1}/I_0, I_{s2}/I_0 and I_{s2}/I_{s1}. Due to the small intensity of the 2.-order sideband (I_{s2}) which brings a big experimental error in evaluating of the integral, only first solution (I_{s1}/I_0) will be considered for evaluating dipolar coupling d_{ij}^{II}.

If the sample has transverse isotropy the similar formula like equation (3.3) can be derived for the ϑ angle dependence. The expansion until 4-th order for such a case can be found elsewhere ([Fil97]).

According to equation (3.3) the dipolar coupling d_{ij}^{II} was calculated combining expression for the 1.-order sideband and the central line in hexamethylbenzene (HMB). MAS spectra of HMB for different rotational frequencies are shown in Figure 3.1. It has to be noted that HMB is not the ideal two spin system sample. The molecule itself rotate very

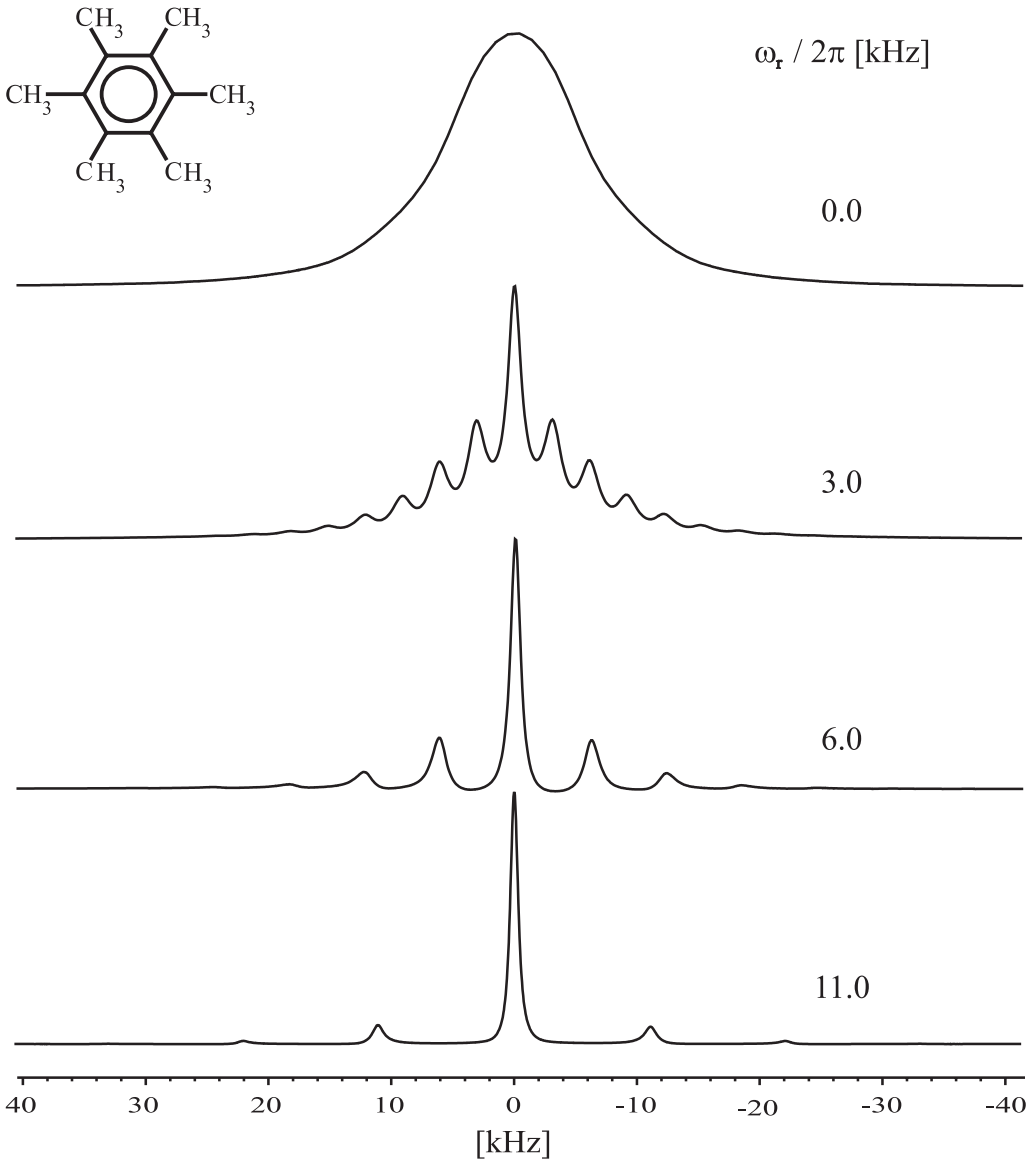

Figure 3.1: *^1H MAS spectra of hexamethylbenzene (HMB) measured at different rotational frequencies ω_r at room temperature. Spectra are normalized to the same amplitude.*

fast and intra-molecular dipolar coupling between protons (^{1}H) in the same molecule are averaged out. Only the spin-spin interactions between molecules (inter-molecular) still remains. Thus, only 'effective' dipolar coupling could be measured. The last spectrum in Figure 3.1, where sample was rotating around the rotor axis under MAS conditions with the frequency $\omega_r/2\pi = 11$ kHz, was chosen to evaluate the coupling. The 'effective' dipolar coupling until the 6-th order approximation was estimated as $d_{ij,ef} = 2\pi \times 8.8$ kHz.

3.2 DQ sideband pattern under MAS

In this section the main difference between δ-pulses sequence (DRAMA/BABA) and spin-lock pulse sequences (C7/POST C7) will be elucidated. Influence of their DQ dipolar average Hamiltonians (see section 2.5.1) on the spin system coupled via dipolar coupling will be studied. We will concentrate on the calculation of the intensities of the DQ coherence which can be used for determining dipolar couplings. Experimental confirmation of the spinning sideband pattern for DRAMA/BABA and C7 will be also presented. Two-dimensional MQ experiment is going to be considered only in this section (see also section 2.5.2).

For deriving DQ intensities at the end of the reconversion period the general form of the zero-order average Hamiltonian for excitation and reconversion period will be used and

$$\hat{\bar{\boldsymbol{H}}}_{DQ}^{exc/rec} = \sum_{i<j} \omega_{ij}^{exc/rec} \hat{\boldsymbol{T}}_{2,2}^{ij} + (\omega_{ij}^{exc/rec})^* \hat{\boldsymbol{T}}_{2,-2}^{ij} \,. \tag{3.4}$$

$\omega_{ij}^{exc/rec}$ in above equation represents the amplitude and the phase of the excitation/reconversion average Hamiltonian (see equations (2.51),(2.52)). In general $\omega_{ij}^{exc/rec}$ is the complex term and it is useful to separate the phase $\Phi_{ij}^{exc/rec}$ and the amplitude $|\omega_{ij}^{exc/rec}|$ variables from it as

$$\omega_{ij}^{exc/rec} = |\omega_{ij}^{exc/rec}|\, e^{i\,\Phi_{ij}^{exc/rec}} \,. \tag{3.5}$$

Detailed calculation for the DQ signal intensity for a two spin-$\frac{1}{2}$ system at the end of the reconversion period was shown in Appendix C and has the form (see equation (C.20)):

$$S_I^{DQ} = \cos(\Phi_{ij}^{rec} - \Phi_{ij}^{exc}) \, \sin(|\omega_{ij}^{rec}|\tau) \, \sin(|\omega_{ij}^{exc}|\tau) \,. \tag{3.6}$$

In addition $|\omega_{ij}^{exc/rec}|$ and $\Phi_{ij}^{exc/rec}$ can depend from Euler angles ϑ and ψ (e.g. see section 2.5.1.1). Presuming the same probability for all angles ϑ,ψ powder average over angles ϑ,ψ has to be performed to get the resulting signal intensity of the DQ coherence S_I^{DQ} in equation (3.6). τ represents an equivalence of the duration of the excitation and reconversion period.

For the moment the phase factor in equation (3.6) inside of the *cos* function will be not regarded because it has no influence to the amplitude of the DQ signal for pulse sequence like DRAMA/BABA as well as for C7 (see sections 3.2.1,3.2.2). In addition let us assume

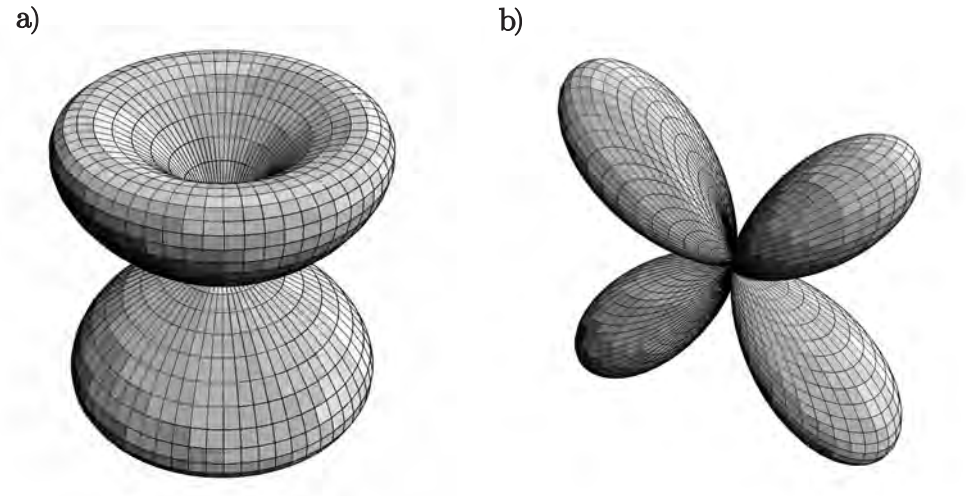

Figure 3.2: *Orientation dependence of DQ intensities from angles ϑ,ψ presented in spherical coordinates for:* a) *C7/POST C7 pulse sequences,* b) *DRAMA/BABA pulse sequences.*

for simplicity $|\omega_{ij}^{rec}| = |\omega_{ij}^{exc}| = |\omega_{ij}(\vartheta,\psi)|$ the DQ intensity gets the form

$$S_I^{DQ} = \left\langle \sin^2(|\omega_{ij}(\vartheta,\psi)|\tau)\right\rangle_{\vartheta,\psi} . \tag{3.7}$$

In the limit of small excitation/reconversion times $\tau \ll |\omega_{ij}(\vartheta,\psi)|^{-1}$ the *sin* function in equation (3.7) can be spread to the Taylor series, where higher orders can be neglected. Separating for convenience $|\omega_{ij}(\vartheta,\psi)|$ to the orientation independent norm $\omega_{ij,norm}$ and angle dependent function $g(\vartheta,\psi)$ where $|g(\vartheta,\psi)| < 1$ the DQ intensity for short time limits is derived and it holds that

$$S_I^{DQ} \simeq \left\langle |g(\vartheta,\psi)|^2\right\rangle_{\vartheta,\psi} \omega_{ij,norm}^2\,\tau^2 . \tag{3.8}$$

The angle dependent functions $|g(\vartheta,\psi)|^2$ for C7 and DRAMA/BABA pulse sequences are shown in Figure 3.2. Equation (3.8) shows us that each pulse sequence is characterized by the average factor $\bar{g}$ which can be derived for DRAMA/BABA pulse sequences (see also section 3.2.1) from[1]

$$\bar{g}^2_{DRAMA/BABA} = \frac{1}{4\pi}\int_0^{\pi} d\vartheta\, \sin(\vartheta) \int_0^{2\pi} d\psi\, \sin^2(2\vartheta)\cos^2(\psi) = \frac{4}{15} \tag{3.9}$$

and for C7 pulse sequence (see also section 3.2.2) from

$$\bar{g}^2_{C7} = \frac{1}{2}\int_0^{\pi} d\vartheta\, \sin(\vartheta)\, \sin^2(2\vartheta) = \frac{8}{15} . \tag{3.10}$$

[1]Powder averaging over angles ϑ,ψ is considered.

Multiplying the average factor $\bar{g}$ with the orientation independent norm $\omega_{ij,norm}$ for particular pulse sequence (see equation (3.8)) effectiveness of the recoupling pulse sequences can be calculated. More details about DRAMA/BABA and C7 will be presented in the next sections.

3.2.1 DRAMA/BABA

It was shown in sections 2.5.1.1 and 2.5.1.2 that DRAMA and BABA pulse sequences can be described by the same zero-order average Hamiltonian. Improved version of BABA pulse sequence acting on the two rotor periods (see Figure 2.17b) has better compensation properties with respect to resonance offsets and small CSA ($||\hat{\boldsymbol{H}}_{CSA}|| \ll ||\hat{\boldsymbol{H}}_{D}||$). The signal intensity just after the detecting pulse in two-dimensional MQ experiment (section 2.5.2) can be assumed as the signal stored in the longitudinal magnetization just after the reconversion period (see also discussion in Appendix C). If in addition so-called total spin coherence ([Wei83, Mun87]) is excited during excitation period all coupled spins are active in MQ coherences and therefore no evolution occurs under the influence of dipolar Hamiltonian (equation (1.59)). Under this conditions signal intensity at the beginning of the detection period ($t_2 = 0$) can be calculated for two spin-$\frac{1}{2}$ system (see equation (3.6) and equation (C.14))

$$S_I(t_1) = \left\langle \cos(|\omega_{ij}^{rec}(t_1)|\tau)\cos(|\omega_{ij}^{exc}|\tau)\right\rangle + \cos(2\Delta\omega_\phi t_1)\left\langle \sin(|\omega_{ij}^{rec}(t_1)|\tau)\sin(|\omega_{ij}^{exc}|\tau)\right\rangle , \tag{3.11}$$

where

$$\omega_{ij}^{exc} = -\frac{3}{\pi\sqrt{2}}\, d_{ij}^{II}\sin(2\vartheta_{ij})\cos(\psi_{ij})e^{-i2\,\Delta\omega_\phi\, t_1} \tag{3.12}$$

$$\omega_{ij}^{rec}(t_1) = -\frac{3}{\pi\sqrt{2}}\, d_{ij}^{II}\sin(2\vartheta_{ij})\,\cos(\psi_{ij}+\omega_r t_1)\,. \tag{3.13}$$

The symbol $\langle\ldots\rangle$ represents the powder average over the angles ϑ, ψ in equation (3.11). Time dependence of the ω_{ij}^{exc} in equation (3.12) is omitted because it appears only in the complex term $e^{-i2\,\Delta\omega_\phi\, t_1}$ and thus is not relevant in its absolute value used in equation (3.11). Nevertheless it influences the phase of the resulting signal described in the *cos* term. τ corresponds to the duration of the excitation/reconversion period and can be only incremented in steps of the rotor period τ_r ($\tau = N\cdot\tau_r$, or $\tau = N\cdot 2\tau_r$ [2]).

[2]For improved version of BABA pulse sequence acting on the two rotor periods (see section 2.5.1.2).

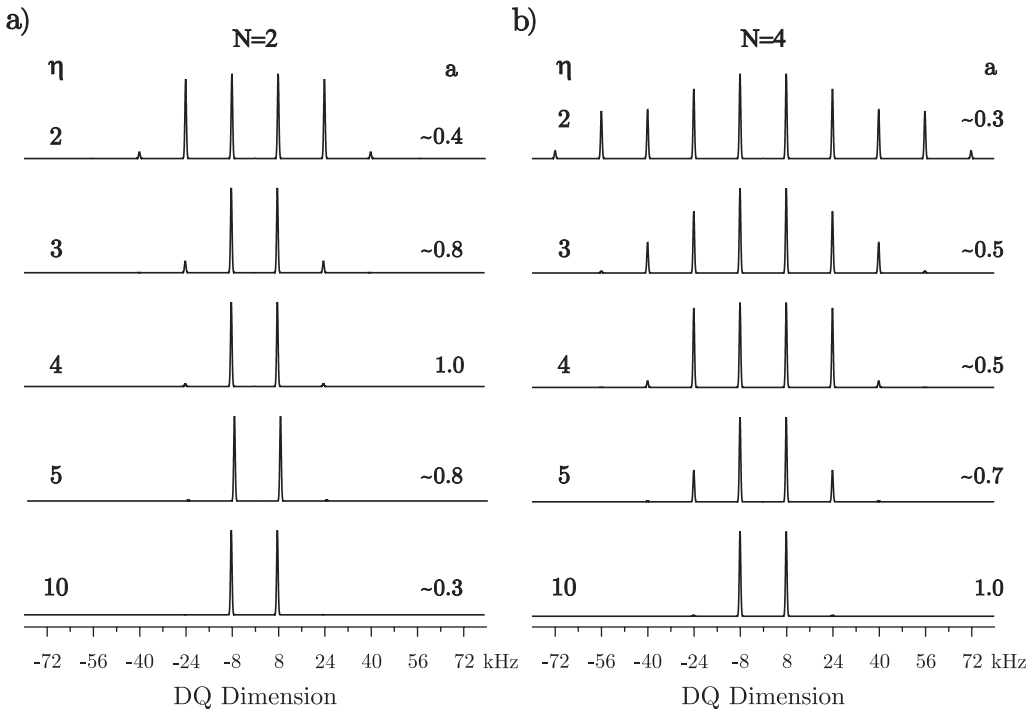

Figure 3.3: *Simulated DQ spinning sideband pattern for DRAMA/BABA pulse sequence for different number of rotor cycles:* a) $N = 2$, b) $N = 4$. *The dependence on the parameter* $\eta = \frac{\omega_r}{d_{ij}}$ *for different coupling strength* d_{ij} *is shown. The relative amplitude of the first DQ sideband is represented by symbol* **a.**

The first term in equation (3.11) describes the rotor-modulated longitudinal magnetization and is usually filtered out from the spectrum (see also section 4.3). The second term is the TPPI-labeled DQ coherence where TPPI-labeling is represented by the phase factor $\Phi_{exc} = 2\,\Delta\omega_\phi\, t_1$. Using Fourier-Bessel series this term can be evaluated ([Got96])

$$S_I^{DQ}(t_1) = \sum_{k=-\infty}^{\infty} \tfrac{1}{2}\Big\{1-(-1)^k\Big\}\left\langle J_k^2\Big(\frac{3}{\pi\sqrt{2}}\;\; d_{ij}^{II}\sin(2\vartheta_{ij})\,\tau\Big)\right\rangle \cos\Big((2\Delta\omega_\phi + k\omega_r)t_1\Big), \quad (3.14)$$

where J_k are the integer-order Bessel functions. The presence of the *cos* factor in equation (3.14) shows that negative and positive frequencies can not be distinguished corresponding to single-channel detection. The argument of the *cos* function describes the separation of the DQ coherence by TPPI procedure. The DQ spectrum is than shifted to the frequency $(2\,\Delta\omega_\phi)/2\pi$ with symmetrically distributed sidebands left from this point at $k \cdot \omega_r$ ($\omega_r = 2\pi f_r$). Hence, a symmetric spinning sideband pattern is generated in indirect t_1 dimension (DQ dimension) with no central line. Only odd-order spinning sidebands at the frequencies $\pm(2k+1)f_r$, ($k \in \boldsymbol{N}$) are present with an intensity modulated by Bessel functions. The relative intensities of the sidebands are determined by the orientation

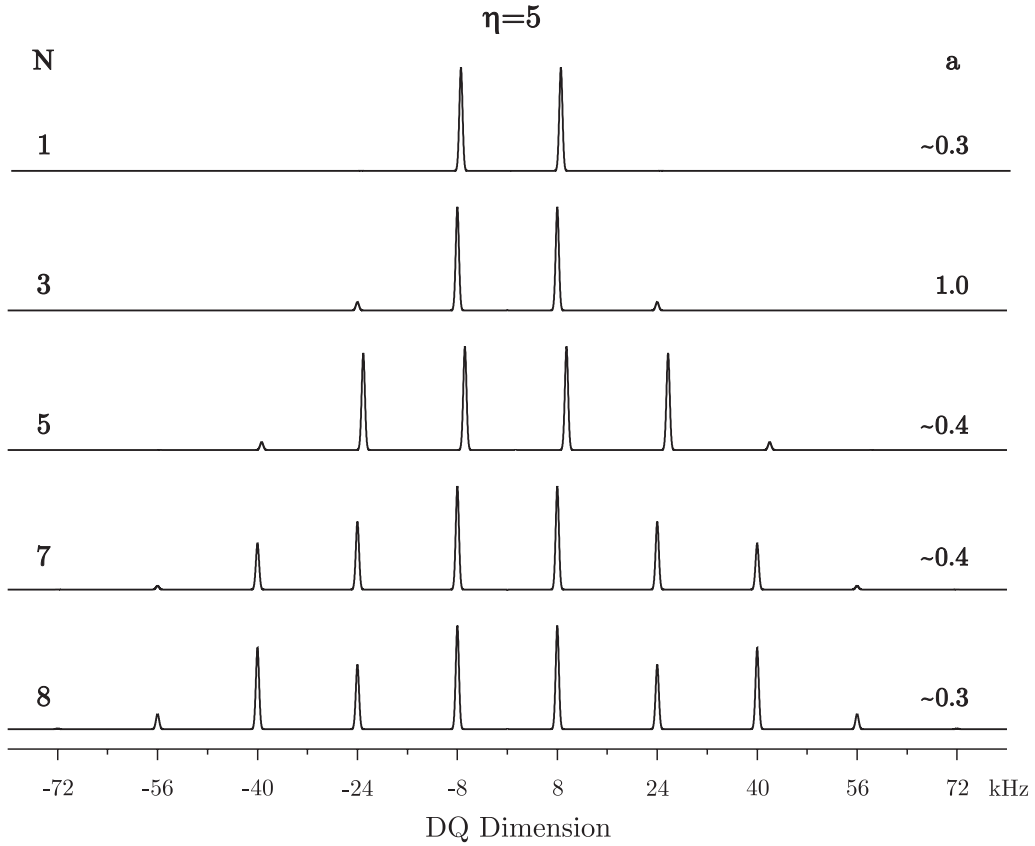

Figure 3.4: *Simulated DQ spinning sideband pattern for different excitation times $\tau = N \cdot \tau_r$. Dipolar coupling strength is chosen 5 times smaller than rotational frequency f_r which corresponds to the dipolar coupling strength $d_{ij} = 2\pi\, 1.6$ kHz for $f_r = 8\, kHz$. More details see description under Figure 3.3.*

and the strength of the dipolar coupling and by duration of the excitation/reconversion period τ.

Simulated spectra of DQ spinning sideband pattern for DRAMA/BABA pulse sequence are shown in Figure 3.3. Isolated spin-½ pairs in a powder have been only considered. Simulations of equation (3.11) (DQ part only) and equation (3.14) showed the conformity for powders as it was expected. The patterns for different excitation time $\tau = N \cdot \frac{1}{f_r}$ of DRAMA and the basic version of BABA pulse sequence are shown in Figure 3.3 as a function of the ratio $\frac{\omega_r}{d_{ij}} = \eta$ (see equation (3.14)) for $N = 2$ and $N = 4$. The powder average is performed numerically. Rotational frequency is chosen $f_r = 8$ kHz. As can be seen from Figures 3.3a and 3.3b number of sidebands are decreasing with increasing η (decreasing the coupling strength d_{ij}) in both cases. For very weak dipolar couplings (or very high spinning speeds) only the first order sidebands govern the spectrum. In

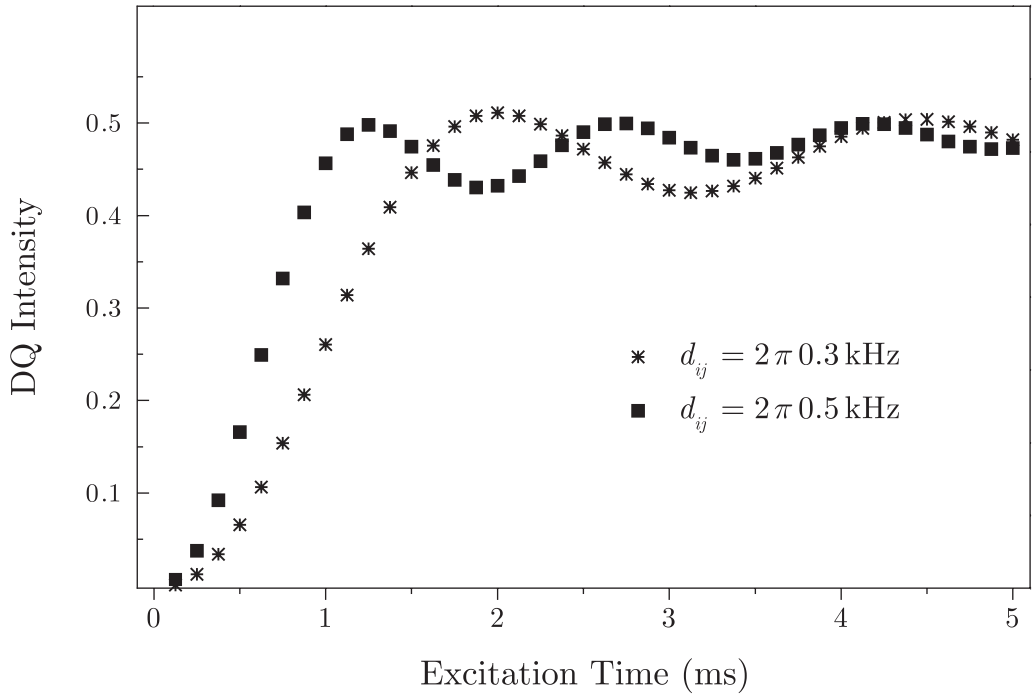

Figure 3.5: *Simulated DQ build-up curves for spin-½ pairs with different dipolar couplings* $d_{ij} = 2\pi\,0.3$ *kHz (asterisks) and* $d_{ij} = 2\pi\,0.5$ *kHz (squares) for DRAMA/BABA pulse sequence. Rotor frequency was chosen* $f_r = 8$ *kHz. The points represent integral intensities of DQ coherence calculated at full rotor periods.*

this regime, the strength of the dipolar coupling is solely reflected in the intensity of this lines and no additional information can be obtained from other spinning sidebands. With increasing number of cycles $N = 4$ (Figure 3.3b) number of sidebands is increasing, thus for very high excitation times one has to expect many sidebands where the probability of overlapping with sidebands from other coherence orders is very high. Growing of the sidebands with increasing excitation/reconcersion time is shown in Figure 3.4. Dipolar coupling was chosen five times smaller than the spinning frequency ($d_{ij} = 2\pi\,1.6$ kHz).

Summing the intensities of the odd-order DQ sidebands up to the sufficient order[3] (equation (3.14)) for different excitation times τ ($\tau = N \cdot \tau_r$) so-called build-up curves can be generated. The simulated DQ build-up curves for spin-½pairs in a powder are presented in Figure 3.5. Comparison of different dipolar coupling strengths for DRAMA/BABA pulse sequence in the regime of fast MAS ($\omega_r \gg d_{ij}$) is presented. The strong dependence on the coupling strength is evident from the figure even for small changes of the coupling. The initial part of the build-up curves can be used for evaluating dipolar coupling strength.

[3]Where the influence of higher orders is negligible.

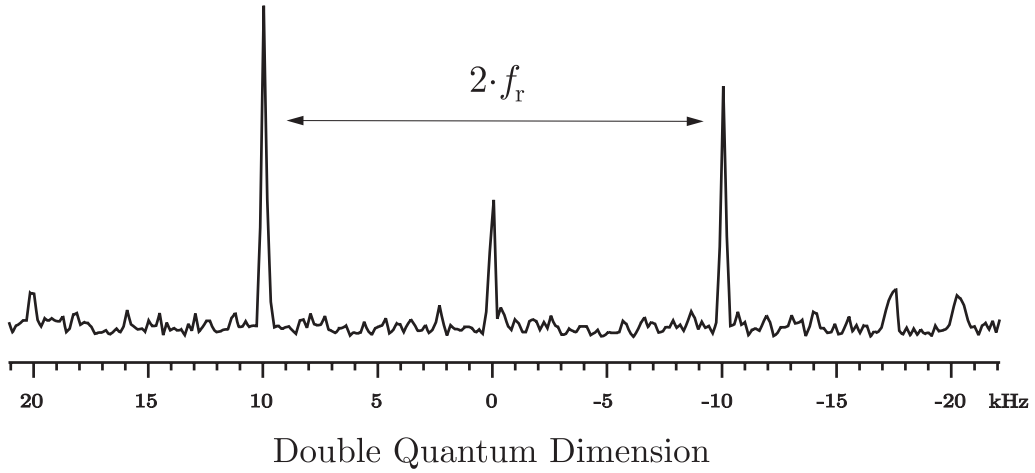

Figure 3.6: *^1H 400 MHz DQ spectrum of polybutadiene melt measured with DRAMA pulse sequence at room temperature. Only the trace which corresponds to the CH_2 group from 2D experiment (more details see section 3.3) was chosen to visualize the appearance of the DQ sidebands. TPPI is performed to separate DQ coherence ($\Delta\omega_\phi = \pi/(4\,\Delta t_1)$; $\Delta t_1 = 12.5\,\mu s$). In addition 32 step DQ filter (see section 4.3) was used to filter out higher order coherences and pulse imperfections. Rotational frequency was chosen $f_r = 10$ kHz and excitation time $\tau = 300\,\mu s$. The length of the $\frac{\pi}{2}$ r.f. pulses was $3\,\mu s$. 20 ms delay after the reconversion period was chosen to allow unwanted transients to decay (see Figure 2.20; $n_0 = 200$).*

Its slope versus the square of the excitation/reconversion time $(N\tau_r)^2$ is proportional to the square of the dipolar coupling d_{ij}^2 (see also equation (3.8)). As can be seen from Figure 3.5 the maximum integral intensity of the DQ coherence can reach about 52% of the initial Zeeman order for a spin-½ pair in a powder. Increasing excitation/reconversion time τ further the DQ coherence exhibits oscillatory behaviour. Experimental results shows (see section 3.3) that this behaviour can not be used for evaluating dipolar couplings. Increasing number of rotor synchronized cycles both the intensity of DQ spectra and the sideband pattern might be influenced by the molecular dynamics and pulse imperfections. Therefore, oscillatory regime will be in most of the cases strongly influenced in real system.

Experimental confirmation of the spinning sidebands pattern is shown in Figure 3.6 for DRAMA pulse sequence. Investigated sample was polybutadiene melt $\{-CH_2 - CH = CH - CH_2-\}$ (more details see section 3.3 and Figure 3.10). Experimental results shows that in the fast spinning regime $f_r = 10$ kHz the first order spinning sidebands dominate the spectrum for protons (^1H) in CH_2 group. In fact this is

only illustrative result that spinning sidebands appear and can not be used for further investigation. Due to the bad compensation property of DRAMA pulse sequence (see section 2.5.1.1) resonance offsets influence the spectrum. Influence of CSA can be neglected for this high spinning regime for this sample. Even after the DQ filtration (see section 4.3) performed in this experiment the rotor modulated magnetization behaving like a zero-quantum coherence (first term in equation (3.11)) is observed in the middle of the spectrum (see Figure 3.6). Influence of the neighboured protons from CH group on the protons in CH_2 group was completely not visible for DRAMA pulse sequence. More details see section 3.3.

Experimental results performed on the same sample with C7 pulse sequence will be presented in the following part.

3.2.2 C7/POST C7

C7 pulse sequence is much more efficient with the comparison to DRAMA and BABA pulse sequences for powders. Improved version called POST C7 is even much less sensitive to the resonance offsets as the original one (more details see section 2.5.1.3). To calculate the signal intensity just after the detecting pulse (see section 2.5.2) zero-order average Hamiltonians for excitation and reconversion period have to be derived, respectively. According to equations (3.4), (2.51) and (2.52) the complex factors $\omega_{ij}^{exc/rec}$ can be estimated for both periods

$$\omega_{ij}^{exc} = \omega_{C7}^{ij}\, e^{-i(2\Delta\omega_\phi t_1 + \psi_{ij})} \qquad \text{and} \qquad \omega_{ij}^{rec} = \omega_{C7}^{ij}\, e^{i(\omega_r t_1 - \psi_{ij})}\,, \tag{3.15}$$

where

$$\omega_{C7}^{ij} = \frac{343(i + e^{i\pi/14})}{520\pi\sqrt{2}}\; d_{ij}^{II}\; \sin(2\vartheta_{ij})\,. \tag{3.16}$$

As can be seen from above relations both ω_{ij}^{exc} and ω_{ij}^{rec} are time t_1 independent in their absolute values which is not the case for DRAMA/BABA pulse sequence (see equations (3.12), (3.13)). Separating the phase and the amplitude variables from equation (3.15) the intensity of the signal ($t_2 = 0$) for system consisting of two coupled spins-½ can be calculated (see equation (3.6) and equation (C.14)) as

$$S_I(t_1) = \Big\langle \cos^2(|\omega_{C7}^{ij}|\tau) \Big\rangle + \cos\Big((2\Delta\omega_\phi + \omega_r)t_1\Big) \Big\langle \sin^2(|\omega_{C7}^{ij}|\tau) \Big\rangle\,, \tag{3.17}$$

where

$$|\omega_{C7}^{ij}| = \frac{343}{520\pi}\; d_{ij}^{II}\; \sin(2\vartheta_{ij}) \sqrt{1 + \sin\frac{\pi}{14}}\,. \tag{3.18}$$

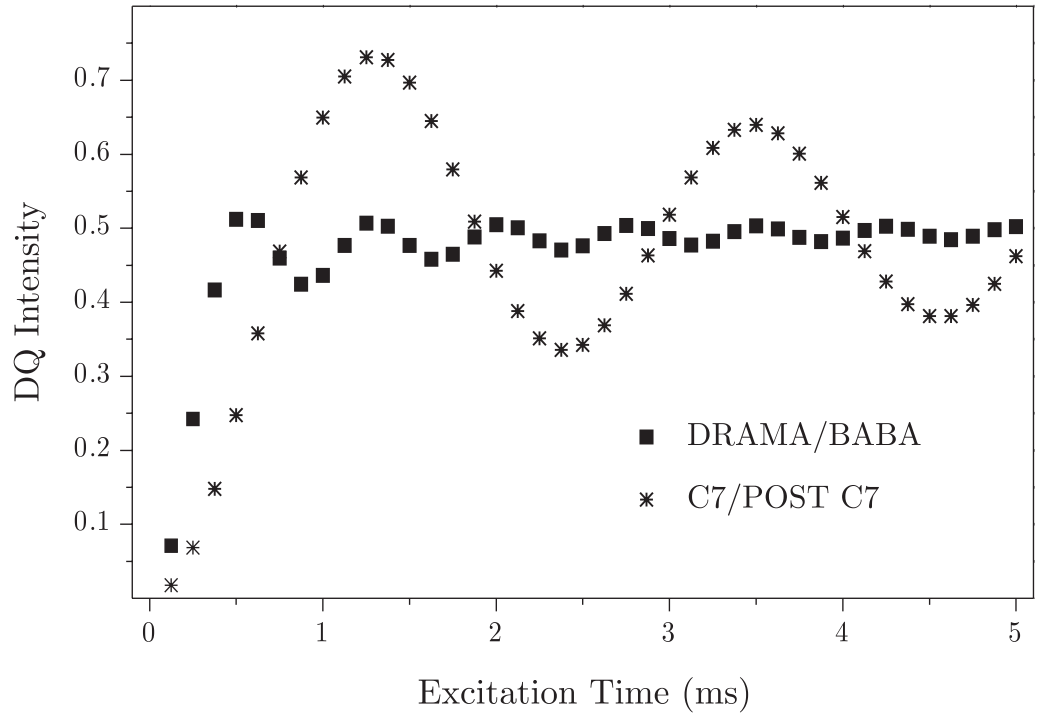

Figure 3.7: *Comparison of the effectiveness of C7/POST C7 (asterisks) and DRAMA/BABA (squares) pulse sequence. DQ build-up curves were simulated for dipolar coupling strength* $d_{ij} = 2\pi\, 1.0$ *kHz and for rotational frequency* $f_r = 8$ *kHz. The points represent integral intensities of the DQ coherence calculated at full rotor periods.*

Averaging over all possible orientations is described by the symbol $\langle \ldots \rangle$ in equation (3.17). Unlike DRAMA and BABA pulse sequences the magnitude of the factor $|\omega_{C7}^{ij}|$ for C7 pulse sequence does not depend on the Euler angle ψ_{ij} (see equation (3.18)), leading to a high overall efficiency for orientationally disordered samples such as powders.

The first term in equation (3.17) describes the remaining part of the initial Zeeman order and has to be filtered out from the resulting spectrum. Despite of DRAMA/BABA pulse sequence (see first term in equation (3.11)) it is not rotor modulated. The second term in equation (3.17) is the most important DQ coherence, modulated by the rotor frequency. Modulation can be seen from the argument of the *cos* function. Orientation dependent norm $|\omega_{C7}^{ij}|$ of the C7 pulse sequence (equation (3.18)) does not depend on the evolution time t_1 hence no spinning sidebands will be seen unlike DRAMA/BABA pulse sequence. Desired DQ signal will be found at the frequency $(2\Delta\omega_\phi + \omega_r)/2\pi$ in indirect dimension (ω_1 dimension), where $\Delta\omega_\phi$ represent the phase shifting of the pulses during excitation period by TPPI procedure (see section 2.5.2). The relative intensity of the DQ

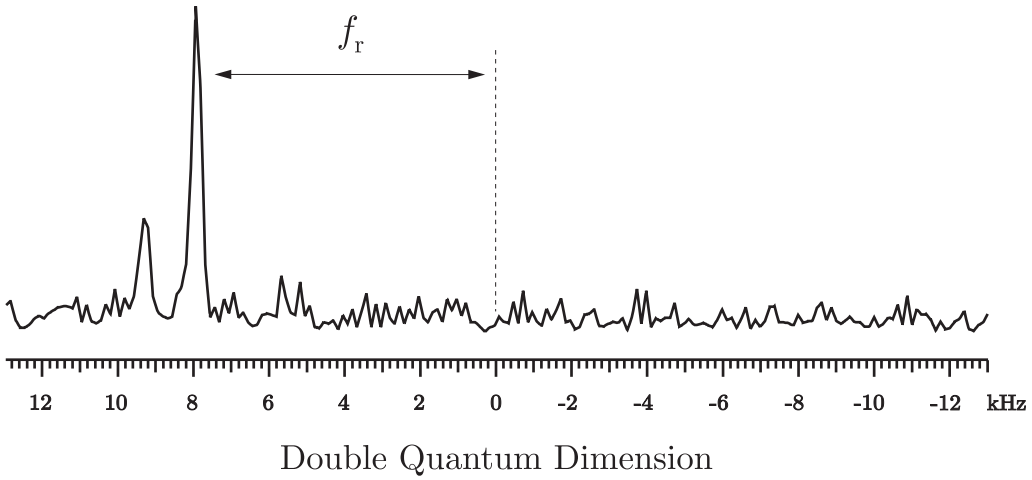

Figure 3.8: *^1H 400 MHz DQ spectrum of polybutadiene melt measured with POST C7 pulse sequence at room temperature. Similar like in Figure 3.6 only the trace corresponding to the frequency of the CH_2 group in ω_2 (direct) dimension is shown. Separation of DQ coherence was made by TPPI so: $\Delta\omega_\phi = \pi/(4\,\Delta t_1)$, $\Delta t_1 = 15.625\,\mu s$. 32 step DQ filter (see section 4.3) was chosen to filter out all unwanted coherences and pulse imperfections. Excitation time τ was set to $500\,\mu s$. Strength of the r.f. pulses was $\omega_{B_1} = 7\omega_r$ ($\omega_{B_1} \simeq 56$ kHz). To allow unwanted transients to decay $15\,\mu s$ delay was inserted between reconversion and detection pulse (see Figure 2.20; $n_0 = 120$).*

signal is determined by the orientation and the strength of the dipolar coupling and by the duration of the excitation/reconversion period (see argument in the *sin* function in equation (3.17)).

Assuming spin-½ pairs in a powder simulation of the DQ build-up curves was performed to compare the effectiveness of C7/POST C7 and DRAMA/BABA pulse sequences. It is shown in Figure 3.7. The maximum DQ integral intensity for C7 pulse sequence is about 73% of the initial Zeeman order, unlike DRAMA where it is only about 52%. For higher excitation times C7 exhibit oscillatory behaviour similar like DRAMA. To evaluate dipolar coupling strength it is enough to regard the initial part of the build-up curve. The slope of this part versus τ^2 is proportional to the square of the dipolar coupling d_{ij}^2 (see equation (3.8)).

DQ spectrum of the polybutadiene melt $\{-CH_2 - CH = CH - CH_2-\}$ with POST C7 pulse sequence is shown in Figure 3.8 similar like for DRAMA pulse sequence (see page 74). Fast spinning regime was chosen with the frequency $f_r = 8$ kHz. The highest peak in the figure corresponds to the strong connectivity between the protons in the CH_2 group. Zero frequency position in Figure 3.8 was set to the frequency related to the TPPI

phase shifting procedure which results for DQ coherence as $2\Delta\omega_\phi/2\pi$. No additional peaks appear in the negative frequency region in the DQ spectrum as was expected. Remaining peak left from the CH_2 group is related to the dipolar coupling between protons in the CH and CH_2 group in polybutadiene which was not observable in the case of DRAMA pulse sequence (see Figure 3.6). Experimental results from POST C7 show much highest effectiveness than from DRAMA pulse sequence. Positive and negative frequencies were clearly distinguished in DQ spectrum which was not the case for DRAMA as well as for BABA pulse sequence. More details will be presented in the next section.

3.3 DQ spectroscopy under MAS

In this section 2D MQ spectroscopy will be explained. As was already mentioned in sections 2.5.2 and 3.2 MQ coherences are detectable in indirect ω_1 dimension. Thus two-dimensional experiment is necessary to perform. The coherences are excited during excitation period (see e.g. Figure 2.20) followed by the evolution period t_1. If so-called total spin coherence is excited MQ coherences does not evolve under the influence of the dipolar Hamiltonian (see equation (2.11)). Nevertheless evolution under the influence of chemical shift interaction is present[4]. In real system pure on-resonance excitation is usually impossible, thus resonance offsets caused by linear interactions like e.g. isotropic chemical shifts or CSA will appear p-times shifted from resonance frequency in ω_1 dimension for each p-quantum coherence (see equation (2.35)). Broadening caused by CSA will be than p-times higher in ω_1 dimension compared to ω_2 dimension. For DQ coherence these frequency shifts (caused by linear interactions) will be twice larger in ω_1 dimension (double quantum dimension) than in ω_2 dimension (single quantum dimension).

In Figure 3.9 the model system of two *functional groups* representing with two chemical shifts ω_A and ω_B is shown. It serves as the intuitive model for understanding DQ coherence. In Figure 3.9a system with two isolated spins is shown. The dipolar coupling between them is very weak and can be neglected. Only DQ coherence between spins within the same group (intragroup coupling) is excited during the excitation period of the pulse sequence and it appears at the frequency positions $2\omega_A$ and $2\omega_B$ in the DQ dimension, respectively. In the single quantum (SQ) dimension frequencies for different groups remains unchanged at positions ω_A and ω_B. In Figure 3.9b a model system is shown for

[4]Other interactions like e.g. J-coupling will be not assumed because they are negligible for our samples.

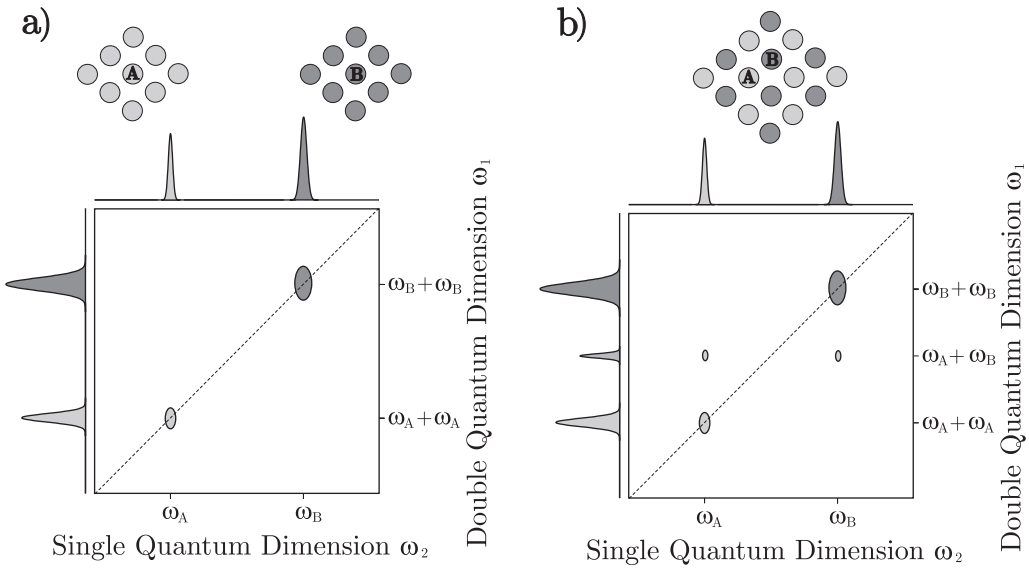

Figure 3.9: *Structure of DQ spectrum for two model systems consisting of two functional groups.*

spins where dipolar coupling between different functional groups is already present (inter-group coupling). This coupling evolves during evolution time with sum of the chemical shifts for both groups and thus appear at the frequency $\omega_A + \omega_B$ in DQ dimension. After reconversion period spins from the different groups carries the original frequency at which they appear in the SQ dimension during detection period. Drawing diagonal line between the coherences appeared from spins originated from the same functional groups, DQ coherences representing the connectivities between this groups appear equally distributed around this line as can be seen from Figure 3.9b.

For demonstrating connectivities between different functional groups the sample of polybutadiene melt was chosen. From the viewpoint of NMR polybutadiene exhibit both liquid-like and solid-like features. At temperatures well about the glass transition temperature dipolar couplings are averaged out by fast molecular motion. However, the presence of topological constrains and permanent crosslinks prevent the chain motion to be free. Thus, dipolar interaction is not completely averaged out and the *residual dipolar coupling* is possible to measure. Our measurements were performed at room temperature which was well above the glass transition temperature ($T_g = 175$K for our sample). At this temperature residual dipolar coupling is scaled in order of 1 kHz which allows us to measure connectivities between groups like e.g. CH and CH_2 in the regime of fast MAS ($\omega_r \gg \omega_D$). Influence of the CSA for our investigated polybutadiene melt will be neglected ($||\hat{\boldsymbol{H}}_{CSA}|| \ll ||\hat{\boldsymbol{H}}_D||$).

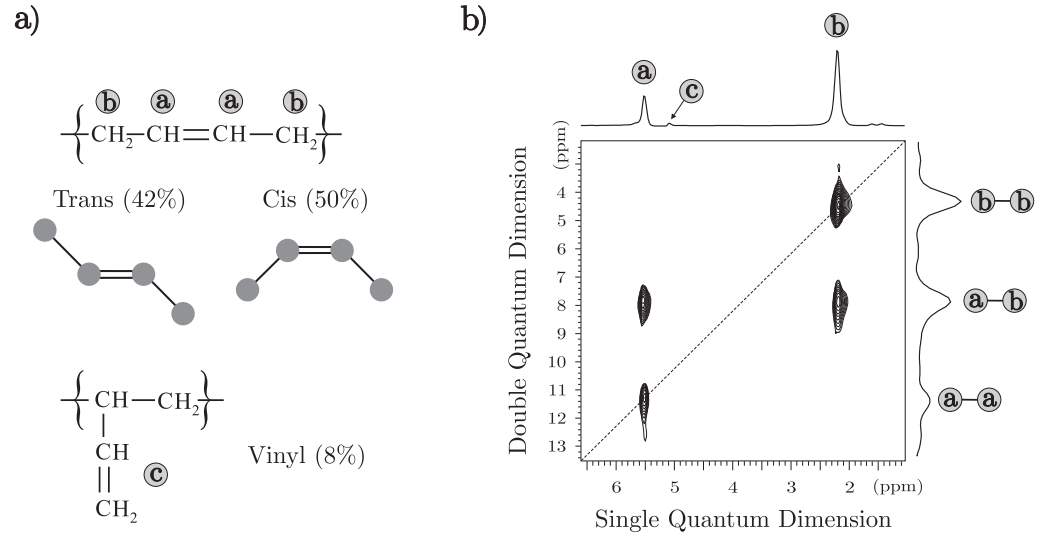

Figure 3.10: *^1H 400 MHz DQ MAS spectrum of polybutadiene melt at room temperature. POST C7 was used at rotor frequency 8 kHz. To separate DQ coherence TPPI phase shifting scheme is performed as in Figure 3.8. Excitation time τ was 1.5 ms to see the maximal DQ signal intensity. A delay 15 ms was included after reconversion period to allow unwanted transients to decay.*

Chemical structure of the polybutadiene melt is shown in Figure 3.10a (M_w=129 000 g/mol, M_n=125 000 g/mol). *Cis* and *Trans* conformations of polybutadiene were not possible to distinguish from our measurements. The spinning speed $f_r = 8$ kHz was not high enough to separate them at the proton frequency $\omega_{0,^1H}/2\pi = 400$ MHz. The percentage of the vinyl butadiene (labeled (c) in Figure 3.10a) was found to be 8% and thus, it was not visible in DQ spectrum (see Figure 3.10b). The SQ projection is found at the top of the DQ spectrum. Experiment qualitatively agree with that made by R. Graf ([Gra97a]). Existence of the peaks in DQ spectrum shows that DQ coherences were established between spins which are relatively close neighbours in space. Only such spins which are close together can contribute to the intensity of the peaks. Dipolar connectivities were found between both groups CH and CH_2. Due to the low intensity of the signal originated from protons (labelled c) in vinyl group connectivities between other groups were not observed. When comparing intensities of different groups one should keep in mind that also the (relative) number of protons of the corresponding group influence them as well as the molecular dynamics. The strongest DQ signal is found between protons inside of CH_2 group (labelled $b-b$) in polybutadiene. Dipolar connectivities between protons from the double bond group ($a-a$) are also visible. Cross-peaks equally distributed from diagonal

line (labelled $a-b$) shows that dipolar coupling between different groups CH and CH_2 is not completely averaged out by fast molecular motion. The cross-peaks indicates that DQ spectroscopy is an unique technique for measuring dipolar connectivities between different groups in polybutadiene melt and thus residual dipolar couplings can be estimated (see section 3.3.1).

For measuring residual dipolar couplings between different and within the same functional groups single DQ experiment presented in Figure 3.10 is still not sufficient. Necessity of more 2D experiment for different excitation/reconversion times is required. Build-up curves has to be generated as will be shown in the next part.

3.3.1 DQ build-up curves

Intensities of DQ coherences were already expressed in sections 3.2.1 and 3.2.2 for DRAMA/BABA and C7/POST C7 pulse sequences, respectively (see DQ part of equations (3.11) and (3.17)). For short excitation times τ this relations, valid for two spin-½ system, can be approximated by parabolic time τ dependence (equation (3.8)). It was shown ([Gra97a]) by computer simulations that this approximative solution can be used even for systems where more spins interact together. In these cases amplitude of the build-up curve is strongly modulated as well as its oscillatory behaviour (see e.g. Figure 3.7). Thus for longer excitation times two spin approximation can not by used. Nevertheless the short excitation time part of the build-up curve can be used for evaluating the dipolar coupling strength. It was simulated ([Gra97a]) that for excitation time $\tau < 0.5\,\frac{2\pi}{d_{ij}}$ for C7/POST C7 pulse sequence ($\tau < 0.25\,\frac{2\pi}{d_{ij}}$ for DRAMA/BABA pulse sequence) the error assuming isolated pairs of spins is less than 10% comparing results from a system where more spins were coupled together. This allow us to use two spin system model in the limit of short excitation and reconversion times. In real experiment equation (3.8) for intensity of the DQ coherence can be in this cases rewritten in the more useful way[5]

$$I_{DQ} \approx A\,\bar{g}^2\,\mathcal{K}_{norm}^2\,(d_{ij}^{II})^2\,\tau^2\,, \tag{3.19}$$

where A represents the instrumental parameter and can not be avoided from an experiment. $\bar{g}$ is the average geometrical factor and together with the norm $\mathcal{K}_{norm}$ of the particular pulse sequence describes their excitation strength. Pulse sequence parameters

[5] $\mathcal{K}_{norm}$ is the dipolar coupling independent norm of the particular pulse sequence, $\mathcal{K}_{norm} = \frac{\omega_{ij,\,norm}}{d_{ij}^{II}}$ (see equation (3.8)).

Pulse Sequence	$\lvert g(\vartheta,\psi)\rvert$	$\mathcal{K}_{norm}$	$\bar{g}\cdot\mathcal{K}_{norm}$
DRAMA/BABA	$\sin(2\vartheta)\cos(\psi)$	$\frac{3}{\pi\sqrt{2}}$	0.348
C7/POST C7	$\sin(2\vartheta)$	$\frac{343}{520\pi}\sqrt{1+\sin\frac{\pi}{14}}$	0.169

Table 3.1: *Excitation strength of the pulse sequences. In the last column powder average is used for calculating average geometrical factor $\bar{g}$.*

$\bar{g}$ and $\mathcal{K}_{norm}$ are listed in Table 3.1. Excitation/reconversion time τ in equation (3.19) can be incremented only in steps of $2\tau_r$ for C7/POST C7 and BABA[6]. In real systems relaxation of spins during excitation as well as during reconversion period has to be taken into account. It can be described approximately through effective relaxation rate T_{eff} and equation (3.19) can be extended as

$$I_{DQ} \approx A\,\bar{g}^2\,\mathcal{K}_{norm}^2\,(d_{ij}^{II})^2\,\tau^2\,e^{-\frac{\tau}{T_{eff}}}\,. \tag{3.20}$$

Experimental factor A plays a crucial role and can not be removed from above equation. As a consequence only relative intensities are possible to measure with the help of build-up curves.

DQ build-up curves measured on the polybutadiene melt which has been already presented in Figure 3.10a are shown in Figure 3.11. Different intensities correspond to the different functional groups as it is indicated. Experimental results show that the strongest coupling comes from the protons in CH_2 group as was expected. Fitting the experimental DQ build-up curves for different functional groups using equation (3.20) the relative values of the residual couplings for different groups can be estimated by[7]

$$\left(D_{CH_2}^{res}\right) : \left(D_{CH_2-CH}^{res}\right) : \left(D_{CH=CH}^{res}\right) = 1.0\ :\ 0.63\ :0.51\,. \tag{3.21}$$

The relative values are scaled to the value of $D_{CH_2}^{res}$. D^{res} represent the scaled dipolar coupling due to the fast molecular motion. Error during the fitting process was 2%, 4% and 6% for each group respectively. It has to be noted that the fitting curves already represent quite big error because we were out of the limit for small excitation times. Thus this fitting errors are not so relevant and they might be even higher for our sample. At

[6]Extended version of BABA is only assumed (see Figure 2.17b). DRAMA and basic version of BABA will be not used because of their bad compensation effects.

[7]We will use the symbol D^{res} instead of d^{II} for residual dipolar coupling.

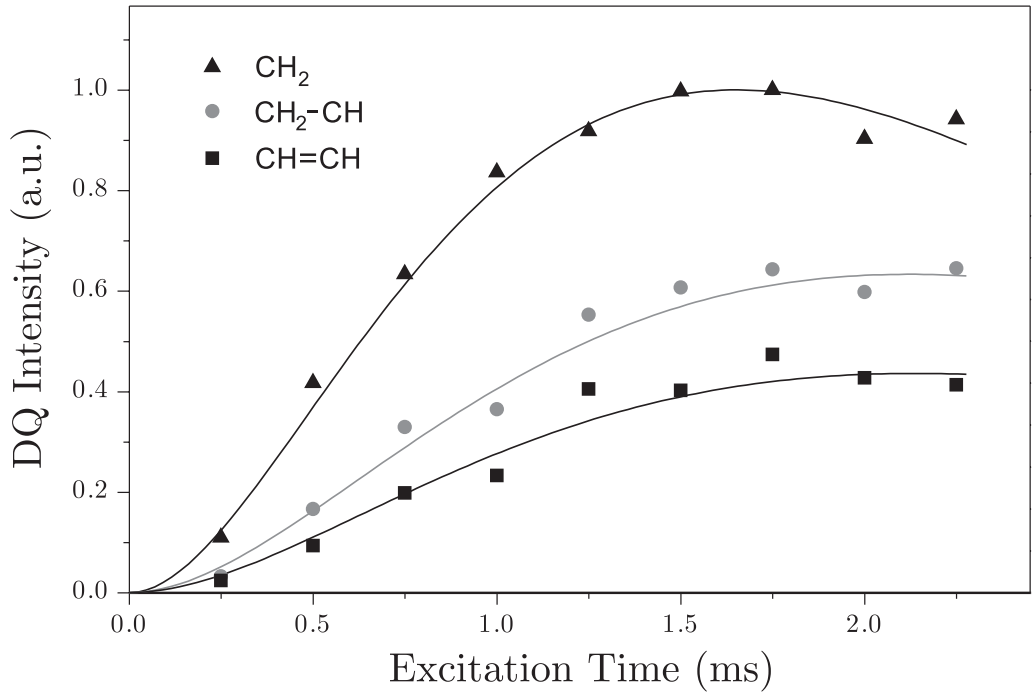

Figure 3.11: *Proton DQ build-up curves for polybutadiene melt measured at room temperature. POST C7 pulse sequence was used to record build-up curves (more details see description under the Figure 3.10). Excitation time was varied in steps of* $2\tau_r$ *(*$\tau_r = 125\ \mu s$*) to achieve full compensation in POST C7 (see section 2.5.1.3). Solid lines represent fitting results from equation (3.20) with fitting parameters* d_{ij}^{II} *and* T_{eff}*.*

this rotor frequency $f_r = 8$ kHz we were not able to distinguish between *Cis* and *Trans* conformations in polybutadiene thus, all values $D^{res}_{CH_2}$, $D^{res}_{CH_2-CH}$ and $D^{res}_{CH=CH}$ represent effective residual dipolar couplings coming from both conformations. To resolve *Cis* from *Trans* conformations from DQ spectra higher rotational frequencies or stronger $\vec{\boldsymbol{B}}_0$ fields are required.

3.3.2 Residual dipolar couplings in natural rubber.

In this section residual dipolar couplings between different functional groups in natural rubber will be measured with the help of ^{1}H DQ spectroscopy. Results from different pulse sequences namely BABA, C7 and POST C7 will be qualitatively compared.

Natural rubber (NR) belongs to the category of elastomers. In elastomers at temperatures well above the glass transition temperature dipolar couplings are much reduced due to the fast molecular motions. However, presence of topological constraints and permanent crosslinks prevent the chain motion to be free so dipolar interactions are not fully

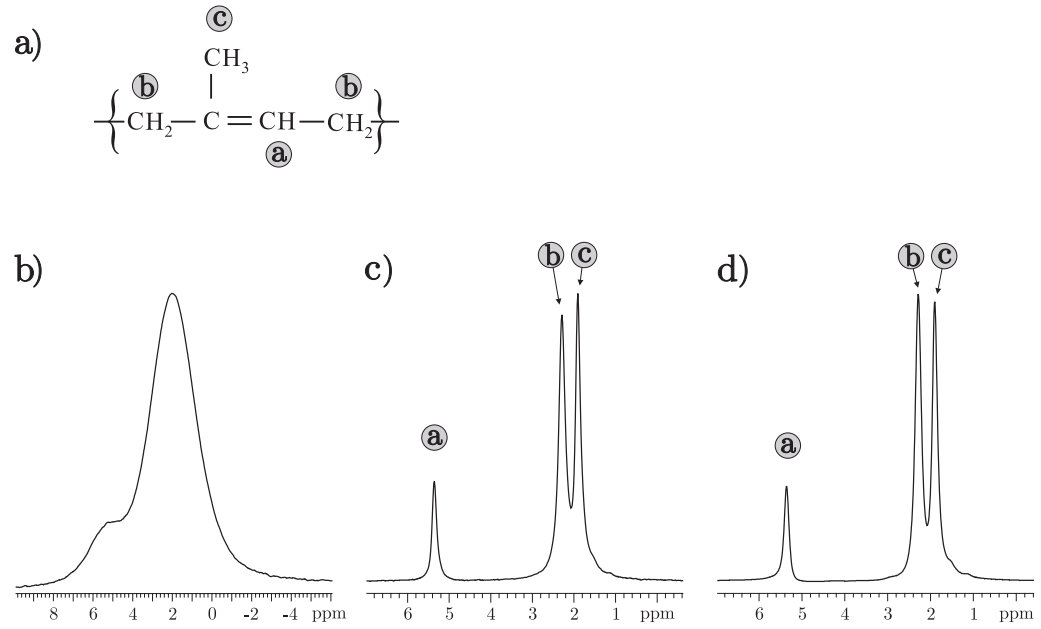

Figure 3.12: *400 MHz ^1H spectra of Natural Rubber with its structure schematically shown in figure* a) *measured at different rotational frequencies namely:* b) $f_r = 0\ Hz$; c) $f_r = 4\ kHz$; d) $f_r = 8\ kHz$.

averaged out. Depending on the degree of motional restrictions, these residual dipolar interactions may be quite small. In NR residual dipolar couplings are scaled on the order of few kHz. This gives rise to measure dipolar connectivities between different functional groups with DQ spectroscopy under the condition of fast MAS.

NR investigated in this section was crosslinked with sulfur (S) in the traditional way where a certain amount of sulfur was added together with an accelerator into the rubber material, before the vulcanization at temperature 150 °C was done. The sulfur and accelerator content was 3.0 phr (*parts-per-hundred rubber*) and 0.54 phr, respectively. The glass transition temperature has been estimated by DSC (*differential scanning calorimetry*) to be $T_g = 208$K. Thus NR was at room temperature (298K) well above the glass transition temperature. From GPC (*gel-permeation chromatography*) molecular mass of the precursor chains was established as $M_w = 850\ 000$ g/mol. Averaged molecular mass of inter-crosslink chains M_c was estimated using uniaxial stress-strain measurements and swelling measurements ([Men99]) as $M_c = 3700$ g/mol.

Measured NR is schematically shown in Figure 3.12a. Three different groups were found with ^{1}H NMR spectroscopy namely CH, CH_2 and CH_3. Spectra at different rotational frequencies are shown in Figure 3.12b−d. Without MAS the three different groups

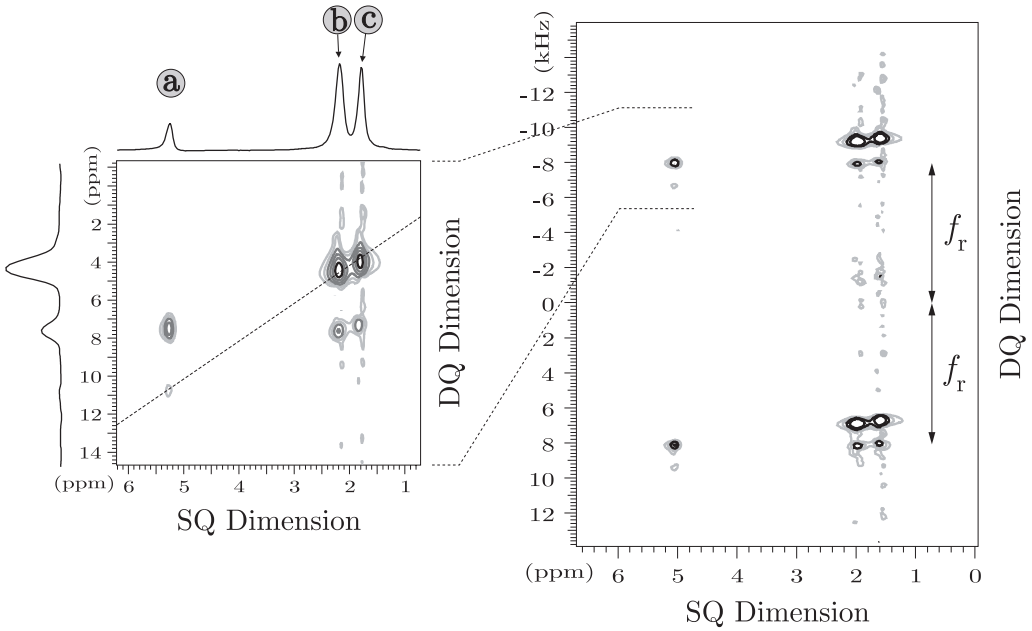

Figure 3.13: ^1H *DQ spectrum of Natural Rubber (Figure 3.12a) acquired with BABA pulse sequence (see Figure 2.17b) at rotor frequency* $f_r = 8$ *kHz. R.f. pulse width was chosen comparable to C7 pulse sequence (see Figure 3.14) as* $t_p = 4.3$ μs*. DQ coherences were excited during excitation period with duration* $\tau = 500$ μs*.*

were not resolved (see Figure 3.12b). Spinning the sample about the rotor axes tilted by 54.7° from the $\vec{\boldsymbol{B}}_0$ field direction additional averaging is introduced. Thus, for high rotational frequencies dipole-dipole coupling as well as CSA[8] are averaged out and only isotropic chemical shift survives (more details see section 1.6). At frequencies 4 kHz and 8 kHz (Figure 3.12c and d) the different groups were almost fully resolved. Comparing figures c) and d) it can be seen that the ratio between CH_2 (labeled (b)) and CH_3 (labeled (c)) group is changed with increasing rotational frequency. This interesting behaviour is most probably caused by better averaging during MAS for protons in CH_2 group than in CH_3 group. CH_2 group is "fixed" to the chain therefore is much less mobile than CH_3 group which is relatively free, hence MAS acting like complementary averaging has stronger influence to the CH_2 group so the line becomes higher and narrower. In addition also intergroup dipolar coupling $(b) - (b)$ (see Figure 3.12a) is averaged out by MAS and can cause similar effects of narrowing of the line corresponding to the CH_2 group.

DQ spectrum of NR is shown in Figure 3.13. BABA pulse sequence was chosen (see Figure 2.17b) to excite DQ coherences at rotational frequency $f_r = 8$ kHz. Clear evidence

[8] Asymmetry part of the chemical shift interaction is not considered (see equation (1.23)).

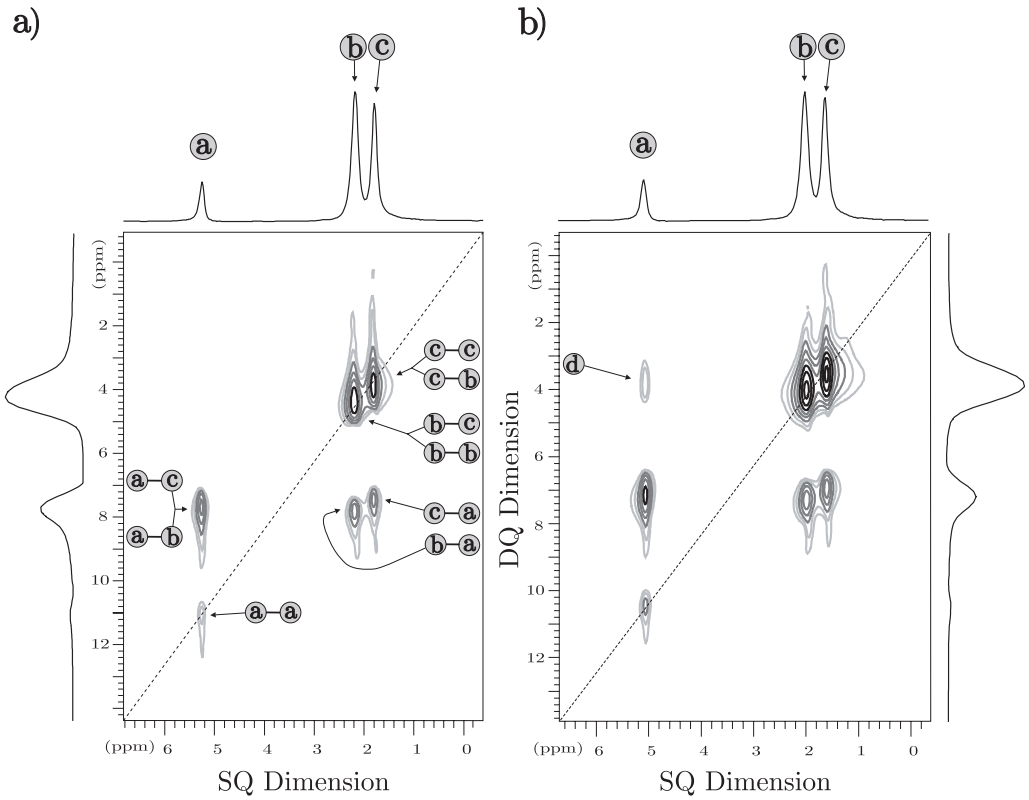

Figure 3.14: *Comparison of effectiveness of C7* a) *and POST C7* b) *pulse sequences. Proton DQ spectra are presented for NR similar like in Figure 3.13 at spinner frequency* $f_r = 8$ *kHz and excitation/reconversion time* $\tau = 1.25$ *ms. Peaks marked* $(a), (b), (c)$ *corresponds to the various functional groups in NR (see Figure 3.12a). Dipolar connectivities between different groups are assigned in DQ dimension as it is indicated. Peak* (d) *represents unwanted magnetization exchange which was established during time* $\tau_0 = 15$ *ms, needed after reconversion period for dephasing unwanted transients.*

of rotational sidebands in DQ dimension can be seen from the right spectrum in Figure 3.13 as was already explained in section 3.2.1. Dipolar connectivities between different functional groups can be seen from the left spectrum in the figure. BABA pulse sequence was not so efficient for exciting DQ coherences. Quite a lot of noise in DQ dimension can be seen in the spectrum. Intensity of the inter-molecular dipolar coupling $CH \leftrightarrow CH$ was hardly resolved from noise. Detailed description of dipolar connectivities between different functional groups can be seen from Figure 3.14a where C7 was used for recording the signal. C7 as well as POST C7 (Figure 3.14b) were much more effective than BABA pulse sequence. It can be directly seen comparing Figures 3.14 and 3.13 that signal to noise in DQ dimension was increased and all possible dipolar couplings were seen as it is indicated

in Figure 3.14a. On the top of the two-dimensional spectra the SQ projections are shown.

Some conclusions can be made from qualitative analysis of the DQ spectra. First of all it has to be noted that we were not able to separate intergroup dipolar coupling $CH_2 \leftrightarrow CH_3$ (labeled as $(c)-(b)$, $(b)-(c)$ in Figure 3.14a) from intragroup couplings between protons of CH_2 ($(b)-(b)$) and CH_3 ($(c)-(c)$) groups. Hence, effective residual dipolar couplings can be only discussed for this groups. Nevertheless dipolar connectivities through space between $CH_2 \leftrightarrow CH$ ($(b)-(a)$) and $CH_3 \leftrightarrow CH$ ($(c)-(a)$) were clearly distinguished in DQ dimension. However, when comparing intensities of the different functional groups, one should keep in mind that (relative) number of protons of the corresponding group has to be also taken into account as well as the molecular dynamics. Assuming only structural parameters DQ signal from CH_3 group is expected to be higher comparing to CH_2 group. However, CH_3 group is relatively free in motion while CH_2 group is "fixed" in the chain which limits its mobility. This results in reduction of the residual dipolar coupling for CH_3 group. Results from POST C7 (see Figure 3.14b) pulse sequence are qualitatively the same as from C7 pulse sequence. In addition peak labeled as (d) appeared which was not the case of C7 pulse sequence. This indicates that the delay between reconversion period and detecting pulse $t_0 = n_0\tau_r$ (see Figure 2.20) for POST C7 during which unwanted transients are supposed to decay was a little bit longer as was necessary. Thus unwanted magnetization exchange between protons of CH_2 and CH as well as CH_3 and CH could be established. Another experiments with shorter τ_0 showed vanishing of this peak which is the confirmation that magnetization exchange took place.

The experimental proton DQ build-up curves for the NR are presented in Figure 3.15. Different categories of functional groups are assigned with symbols $A, B, \ldots, E$ as it is indicated in the left part of the figure. Series of two-dimensional experiments at different excitation times with POST C7 pulse sequence were performed to record the signal. As was already mentioned we were not able to resolve all couplings from the experiment thus, symbols A and B corresponds to the overall residual couplings as it is indicated in the figure. Due to the fast axial rotation of the CH_3 group around three fold axis the proton dipolar coupling is reduced by the factor of $\frac{1}{2}$ compared to the rigid case ([Sch99]). This is the main reason why residual dipolar coupling of the CH_3 group is reduced such that it is a little bit lower than residual dipolar coupling of the CH_2 group (compare intensities B and A in Figure 3.15). As a consequence of existence of crosslinks between chains, intermolecular dipolar coupling between protons of $CH \leftrightarrow CH$ (labeled as E) of neighboured

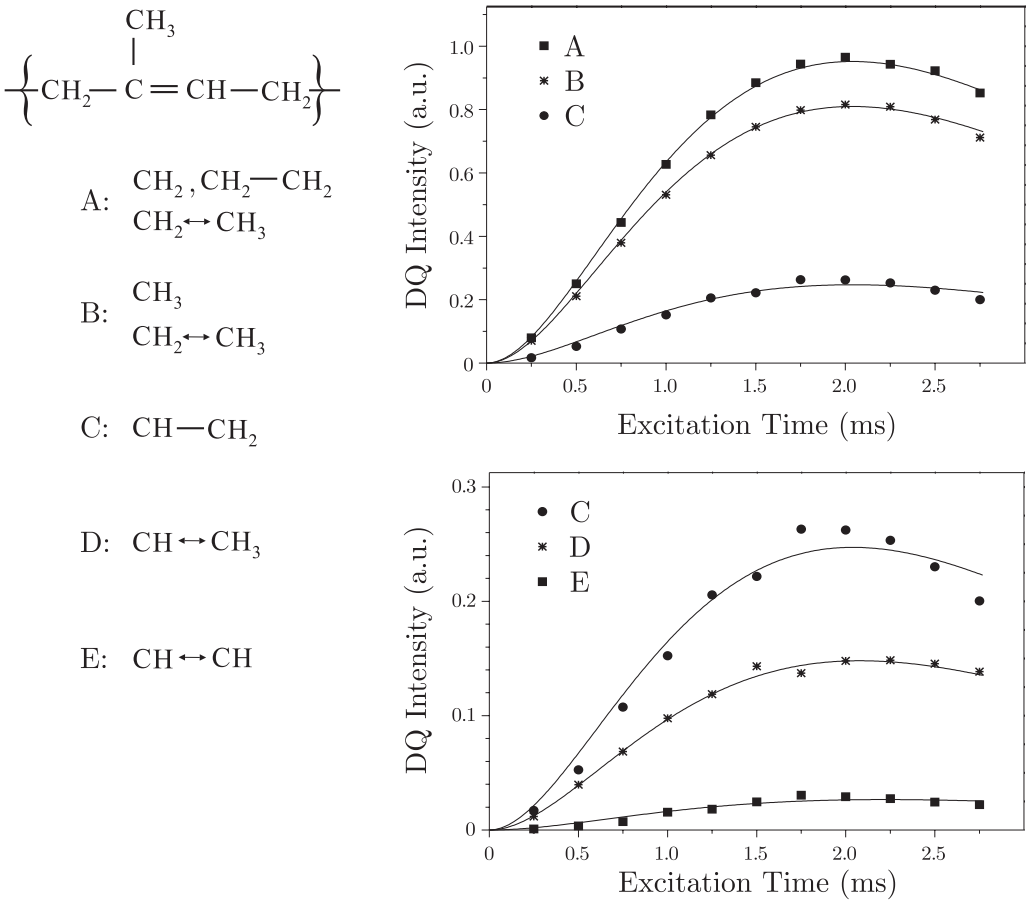

Figure 3.15: ^1H *DQ build-up curves of NR recorded with POST C7 pulse sequence (Figure 2.19b). Symbols* $A, \ldots, E$ *corresponds to the dipolar connectivities between different groups as it is indicated in the left part of the figure. Solid lines represent fitting curves (more details see text).*

chains[9] is not fully averaged out. As expected this residual dipolar coupling was found to be smallest. Equation (3.20) was used to fit experimental DQ build-up curves for different groups. Due to the unknown experimental factor A of that equation only relative values of residual couplings D^{res} could be calculated. Fitting results

$$(D_A^{res}) : (D_B^{res}) : (D_C^{res}) : (D_D^{res}) : (D_E^{res}) = 1.0 \ : \ 0.92 \ : \ 0.51 \ : \ 0.38 \ : \ 0.15 \qquad (3.22)$$

are normalized to the maximal value of the residual coupling D_A^{res} found in the spectrum. Fitting errors were calculated for A, ..., E respectively as 1%, 1%, 2%, 4%, 8%. Similar like in section 3.3.1 these error values are not so relevant and can be even higher for our sample.

[9] Also coupling between protons from the same chain might contribute to the resulting intensity of the DQ signal labeled as E.

Absolute values of residual dipolar coupling which may be estimated from the first order spinning sidebands in SQ MAS experiment (see section 3.1) were not possible to be measured due to the non-symmetrical spinning sidebands. This asymmetry might be caused by spectrometer problems or by presence of CSA. Therefore more detailed analysis of NR were not made. Nevertheless it was shown that ^{1}H DQ spectroscopy permits site-selective measurements of residual dipolar couplings between protons belonging to the same or to the different functional groups even for more complicated structures like NR. To resolve all dipolar connectivities higher rotational speeds or stronger $\vec{\boldsymbol{B}}_0$ fields are required which was not available.

3.4 Spin counting under MAS

Experimental results from spin counting experiment will be shown in this section. Theoretical bases can be found in section 2.5.3. Adamantane was used as a test sample to excite higher order coherences under MAS. As was already explained in section 2.5.3 no evolution of the spin system in spin counting experiment take place on contrary to the DQ spectroscopy (see section 3.3) thus, no spinning sidebands are expected in second dimension. POST C7 will be used to excite multiple quantum (MQ) coherences. Only even quantum coherences will be expected because POST C7 is described by 'pure' DQ Hamiltonian for two spin-$\frac{1}{2}$ system ([War80]).

Experimental results from MQ spin counting experiment made on Adamantane are shown in Figure 3.16. Adamantane represents a relatively strong coupled spin system (more details see page 45) where higher order coherences can be expected. Experiment was carried out at MAS frequency $f_r = 8$ kHz. Two different excitation times τ were chosen to demonstrate the effect of dynamics of the MQ coherences. Increasing excitation time higher order coherences were exited with POST C7 pulse sequence as was expected (compare Figure 3.16a and b). MQ coherences are modulated by $\cos(p\,\Delta\phi \cdot m)$ (see [Shy88] and section 2.5.3) therefore Fourier transformation with respect to m (representing second dimension) give rise to a series of δ-function spikes corresponding to the MQ coherence order p. Separation of different quantum orders is accomplished by $\Delta\phi$. Up to the 14-th order of coherences were clearly visible in Adamantane with excitation time $\tau = 1$ ms (Figure 3.16b) recording the signal with this phase incremented method.

Effective size of the dipole-dipole coupled spin clusters $N(\tau)$ for given

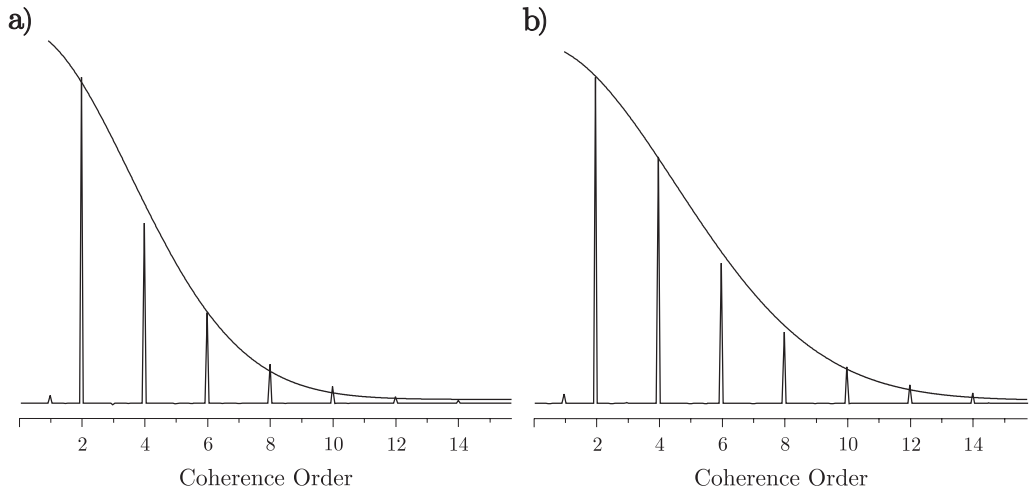

Figure 3.16: ^1H *MAS spin counting MQ experiment for Adamantane at rotational frequency* $f_r = 8$ *kHz. POST C7 was chosen to excite MQ coherences. Two different excitation times* a) $\tau = 750$ μs *and* b) $\tau = 1$ *ms corresponding to complete multiples of rotor period were used to visualize growing of higher order coherences. DQ coherence is normalized to the same amplitude for both experiments. Solid lines represent the fitting curve for evaluating sizes of the spin clusters* $N(\tau)$ *by equation (3.23).* $\Delta\phi$ *was chosen* $11.25°$ *to see up to the 16-th order (*$p_{max} = 16$*) of coherence. Only 32 phase increments were recorded which correspond to the full* 2π *cycle. 1 ms delay (*τ_0*) was included after reconversion period to allow unwanted transients to decay.*

excitation/reconversion time τ can be extracted from spin counting experiment by assuming that the intensity of p-quantum coherence is related to the number of different transitions of order p in a system of $N(\tau)$ spins. These can be calculated directly from combinatorial arguments which can then be approximated by a Gaussian distribution ([Bau85]) for large clusters $N(\tau) \geq 6$. Hence, MQ intensities can be fitted by Gaussian distribution of the form ([Bau86, Shy88])

$$I_{MQ}(p,\tau) = A \exp\left(\frac{-p^2}{N(\tau)}\right) \tag{3.23}$$

with variance $\sigma^2 = N(\tau)/2$, where A is normalization constant and $N(\tau)$ is the cluster size which develops over the time τ. Solid lines plotted over the intensities of MQ coherences in Figure 3.16 represent fitting curves by equation (3.23). Fitting results $N(750\mu\text{s}) = 24.7 \pm 2.0$ and $N(1\,\text{ms}) = 41.2 \pm 1.7$ shows increasing amount of correlated spins as was expected. Results are in a good agreement with R. Graf measurements ([Gra97a]), where C7 pulse sequence was used.

It is important to note that in spin counting experiment the linewidth information from the second dimension is eliminated which is not always desired. However, when

MQ intensities are required, rather than lineshape information, spin counting experiment provides a sensitive and much less time consuming experiment than conventional two-dimensional MQ experiment where t_1 is incremented in the sense of TPPI as was presented in section 2.5.2. In the case of Adamantane where resonance offsets are negligible also incomplete cycles ([Gee99]) can be used for exciting higher order coherences with C7 pulse sequence. Care has to be taken when more isotropic lines can be resolved by MAS. Full compensation of resonance offsets and r.f. field inhomogeneities is accomplished only after complete 7-fold cycles (multiples of twice rotor period) in C7 as well as in POST C7 pulse sequence ([Lee95, Hoh98]) so incomplete cycles are not desired in these cases when on resonance excitation is impossible.

3.5 MQ coherences for static solids

In this section a quantitative comparison of eight pulse sequence (see section 2.4.1.2) and thirty-two pulse sequence (see sections 2.4.1.3) will be made. DQ build-up curves for static solids where dipolar couplings are relatively weak (in the order of few kHz) will be presented for both pulse sequences. Comparison with high resolution MAS (see section 3.3.1) will be also discussed. In the second part of this section MQ spin counting experiment with thirty-two pulses sequence will be described. Up to the 6-th order of coherences were observed in polybutadiene rubber. Two samples were chosen to accomplish experiments.

The first one was polybutadiene melt (PBM) (see Figure 3.17a,b) already described in section 3.3 (see page 79 and Figure 3.10). MAS spectrum recorded at rotational frequency $f_r = 3$ kHz is shown in Figure 3.17b. At this spinning frequency both groups CH and CH_2 were clearly resolved. The vinyl group (Figure 3.17b labelled as c) was much smaller than another isotropic lines so its influence to the resulting integral in static experiment in Figure 3.17a is less than 10% so it will be neglected. PBM will be used in section 3.5.1.

The second sample was polybutadiene rubber (PBR) with a high crosslink density. It is based on a commercial *cis*–1,4 polybutadiene (BUNA *cis* 132) with $M_n = 120\,000$ g/mol and $M_w = 450\,000$ g/mol. Crosslinking has been done with dicumyl peroxide (DCP) in the traditional way where DCP was mixed with the rubber material, before the vulcanization process at temperature 145 °C during 1 h with pressure 10 MPa was performed. The resulting mean molecular mass between two crosslinks, $M_c = 6500$ g/mol ([Eka00]), was determined as the average value from stress-strain measurements [Mat92], swelling

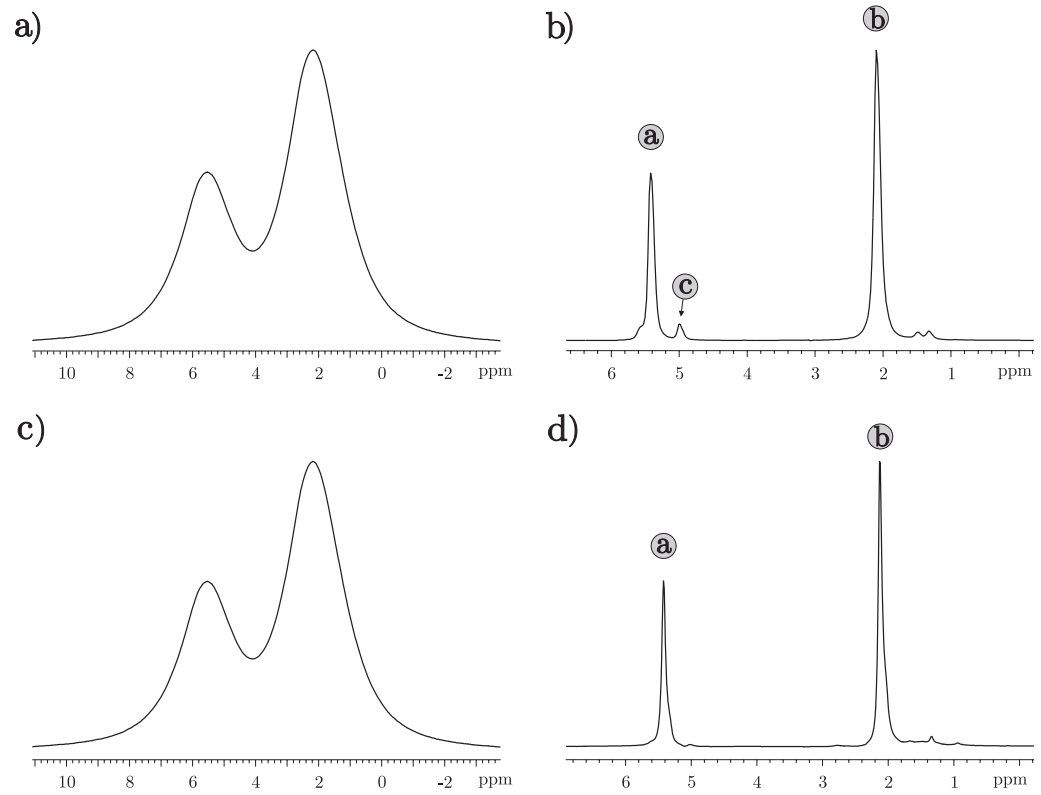

Figure 3.17: *Proton ^1H spectra measured at rotational frequencies $f_r = 0$ Hz for* a), c) *and $f_r = 3$ kHz for* b), d). *Two different samples were measured:* a), b) *polybutadiene melt (PBM);* c), d) *polybutadiene rubber (PBR). Labels* a,b,c *correspond to the different groups resolved by MAS (see Figure 3.10a).*

measurements ([Lec93]) and NMR relaxation measurements ([Sim92]). Free chains of polybutadiene melt with $M_n = 1800$ g/mol were incorporated into the rubber network with weight amount of 20% (wt.%) ([Eka00]). Originally two effects due to this incorporation were expected. The first one is like swelling and should give rise for small swelling degrees to a better mobility. For large swelling degrees the mobility can decrease again ([Men99, Sch89]). The second effect could results in additional topological hindrances due to the comparable incorporated free chain length with the size of the entanglement chain length. This should increase the residual coupling (decrease mobility). But after this incorporation procedure rubber network appears extremely rigid. The mechanical properties were extremely worse (it breaks immediately), which was not expected. The most possible cause for this behaviour is additional crosslinking of the short free chains inside the original sample, which result in extremely high crosslinked piece of the sample. As a check measurement the resulting mean molecular mass between two crosslinks after

incorporation was measured again with ^1H Hahn-Echo experiment ([Men99, Sim92]) as $M_c = 700$ g/mol. This high crosslinking density can increase the probability to observe higher order coherences in PBR. Glass temperature of PBR was estimated from DSC (*differential scanning calorimetry*) to be $T_g = 168$K. Proton NMR spectra of PBR at $f_r = 0$ kHz and $f_r = 3$ kHz are shown in Figure 3.17c and 3.17d, respectively. Comparing Figure 3.17a with Figure 3.17b not so much differences can be seen. PBR will be used as a test sample in section 3.5.2 to observe higher order coherences.

3.5.1 DQ build-up curves of polybutadiene melt

Similar formalism like for C7 and DRAMA/BABA pulse sequences (see sections 3.2.1 and 3.2.2) can be used for calculating intensities of the signal arising from dipolar coupled two spins ½ for eight pulse sequence as well as for thirty-two pulse sequence (more details see Appendix C and e.g. section 3.2.1 or section 3.2.2). To derive DQ average Hamiltonians during excitation and reconversion periods equations (2.51) and (2.52) (or equations (2.53) and (2.54)) can be used, respectively. With the help of equation (2.34) which represents zero-order average Hamiltonian for both pulse sequences for a system of spins-½coupled via dipole-dipole interaction, factors $\omega_{ij}^{exc/rec}$ (see section 3.2) can be estimated for excitation as well as for reconversion period[10]:

$$\omega_{ij}^{exc} = D_{ij}\, e^{-2\phi} \qquad \text{and} \qquad \omega_{ij}^{rec} = D_{ij}\,, \tag{3.24}$$

where

$$D_{ij} = d_{ij}^{II}\ \tfrac{1}{2}\left(3\cos^2\vartheta_{ij} - 1\right)\,. \tag{3.25}$$

ϕ corresponds to the phase shifting of the pulses during excitation period and can be $\phi = \Delta\omega_\phi\, t_1$ for TPPI MQ experiment (see section 2.4.3) or $\phi = m \cdot \Delta\phi$ for spin counting MQ experiment (see section 2.4.4).

The phase and the amplitude can be separated from equation (3.24) and for dipolar coupled spin-½ pair the signal intensity arising from this coupling can be calculated for $t_2 = 0$ (see equation (C.20) and equation (C.14)) as

$$S_I(\phi) = \left\langle \cos^2(D_{ij}\,\tau)\right\rangle + \cos(2\phi)\left\langle \sin^2(D_{ij}\,\tau)\right\rangle\,. \tag{3.26}$$

Averaging over all possible orientations is described by the symbol $\langle\ldots\rangle$. The first term in equation (3.26) similar like for C7 and DRAMA/BABA pulse sequences represents

[10] More details see section 2.5.2 or section 2.5.3.

Pulse Sequence	$\lvert g(\vartheta,\psi)\rvert$	$\mathcal{K}_{norm}$	$\bar{g}\cdot\mathcal{K}_{norm}$
8p/32p	$\frac{1}{2}\,(3\,\cos^2\vartheta-1)$	1	0.447
DRAMA/BABA	$\sin(2\vartheta)\cos(\psi)$	$\frac{3}{\pi\sqrt{2}}$	0.348

Table 3.2: *Comparison of excitation strengths of eight (8p) and thirty-two (32p) pulse sequence with DRAMA/BABA pulse sequence. In the last column powder average is used for calculating average geometrical factor $\bar{g}$ (see e.g. equation (3.9)).*

remaining part from the initial magnetization. It can be filtered out from the spectrum by conventional double quantum (DQ) filter (see section 4.3). DQ part of the signal is described by the second term in equation (C.14). The first term of the DQ signal ($\cos(2\phi)$) carries information about the phase and only the second *sin* term represents the intensity of the DQ signal.

In the limit of short excitation and reconversion times τ the intensity of DQ signal (see *sin* part of equation (3.26)) can be approximated by quadratic dependence on τ (more details see section 3.3.1). Assuming relaxation of the spin system during excitation/reconversion period described through T_{eff} the DQ intensity can be written in the form

$$I_{DQ} \simeq A\,\bar{g}^2\,\mathcal{K}^2_{norm}\,(d^{II}_{ij})^2\,\tau^2\,e^{-\frac{\tau}{T_{eff}}}\,. \tag{3.27}$$

Average geometrical parameter $\bar{g}$ and orientation independent norm $\mathcal{K}_{norm}$ for eight pulse sequence as well as for thirty-two pulse sequence are listed in Table 3.2. Comparison with DRAMA/BABA pulse sequence (Table 3.1) is also shown. Simulation of the DQ intensities from equation (3.26) shows (performed numerically with home made program) that maximum DQ intensity for powders is about 61% of the initial Zeeman order which is even higher than for DRAMA/BABA pulse sequence where it was about 52% (see section 3.2.1). Disadvantage of eight and thirty-two pulse sequences are their low resolution capabilities in comparison to pulse sequences working under MAS. Nevertheless if high resolution is not required static MQ pulse sequences can be sometimes preferred. Their excitation/reconversion time τ is not rotor synchronized in spite of C7 as well as BABA/BRAMA pulse sequences, which is an advantage in some cases when high speed MAS is not available and beginning part of the build-up curve has to be recorder with higher accuracy.

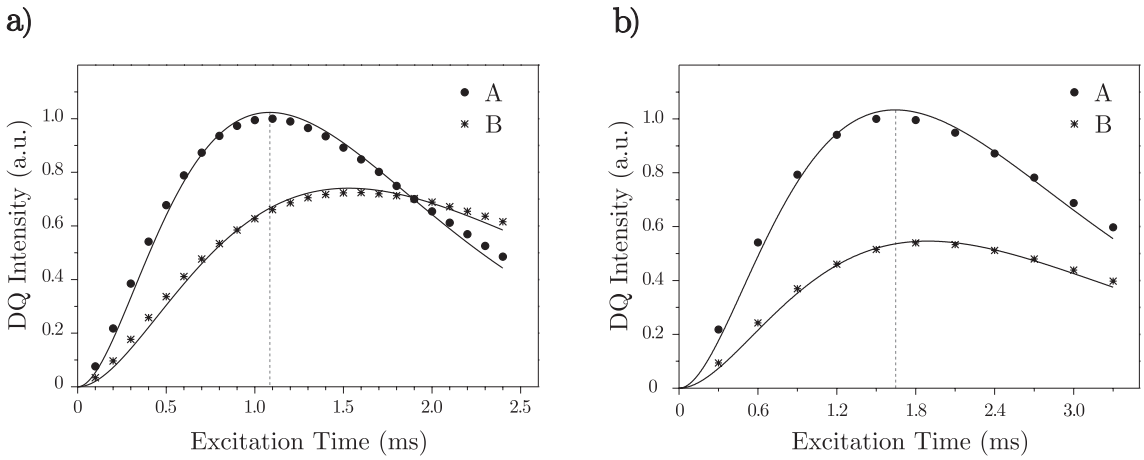

Figure 3.18: *Comparison of 1D DQ build-up curves between eight pulse sequence* a) *and thirty two pulse sequence* b) *for polybutadiene melt (PBM). Experiment was carried out at 400 MHz Larmor frequency for protons* ^1H*. Solid lines represent fitting curves by equation (3.27). The vertical dashed lines mark the excitation times for maximum signal for the protons of group A, which differs for each pulse sequence. The group A symbolized DQ signal corresponding to the* $-CH_2-$ *and* $CH_2 - CH$ *couplings and the group B to* $CH_2 - CH$ *and* $CH = CH$ *couplings. The cycle time* τ_c *was* 100 μs *(*$t_p = 3.4$ μs, $\Delta = 4.9$ μs *and* $\Delta' = 13.2$ μs*) for* a) *and* 300 μs *(*$t_p = 3.4$ μs, $\Delta = 21.6$ μs *and* $\Delta' = 46.6$ μs*) for* b)*, respectively (see sections 2.4.1.2 and 2.4.1.3). A delay of* $\tau_0 = 4$ *ms was included after reconversion period to allow unwanted transients to decay away from the spectrum.*

DQ build-up curves for eight pulse sequence (see Figure 2.10b) and for thirty-two pulse sequence (see Figure 2.11) are shown in Figure 3.18. As was already mentioned polybutadiene melt (PBM) was chosen (see Figure 3.17a). Performing double quantum filtration (DQF) in equation (3.26) (see section 4.3) the first term can be filtered out from the spectrum and only DQ term survives[11]. For PBM higher order coherences are low probable due to its high mobility. Thus, DQF is sufficient to filter out all unwanted coherences. This kind of experiment was performed in Figure 3.18 while time t_1 between excitation and reconversion period was zero ($t_1 = 0$) and only excitation/reconversion time τ was incremented. This experiment will be called one dimensional (1D) DQ experiment. The main drawback of 1D DQ is that it is no able to resolve dipolar couplings between different groups (intergroup coupling). Hence, we were not able to resolve the dipolar coupling $CH - CH_2$. In comparison with two-dimensional (2D) DQ experiment (see

[11]This assumption can be made only in the limit of relatively short excitation and reconversion times τ, where higher order coherences $(6, 10, \ldots$-orders) are not expected.

Figure 3.11) 1D DQ experiment provides less information. Nevertheless 1D DQ experiment is much less time consuming, hence full build-up curves can be obtained in couple of hours which is not the case of 2D MQ experiment.

Comparing Figures 3.18a and 3.18b the different relaxation rates of the spin system during excitation/reconversion period can be directly seen (compare e.g. excitation times belonging to the vertical dashed lines in the figure). For eight pulse sequence (Figure 3.18a) even the relaxation rates for different groups (labeled A and B in the figure) are seen. The origin of this behaviour might be in insufficient compensation of isotropic chemical shifts for eight pulse sequence (see also section 2.4.1.2). Higher order terms in average Hamiltonian in Magnus expansion (section 1.3) can influence the spectrum, thus, with increasing excitation time τ the error is rising for eight pulse sequence. Thirty-two pulse sequence on the other hand provides better compensation of resonance offsets so this spurious effects are not seen (see Figure 3.18). Nevertheless the initial part of the build-up curves can be used for fitting to obtain residual dipolar couplings for different groups A and B also for eight pulse sequence. Equation (3.27) was used for fitting 1D DQ build-up curves for both pulse sequences (solid lines in Figure 3.18) with the result

$$\left(D^{res}_{8p,A}\right) : \left(D^{res}_{8p,B}\right) = 1.0 : 0.60 \qquad \text{and} \qquad \left(D^{res}_{24p,A}\right) : \left(D^{res}_{24p,B}\right) = 1.0 : 0.63\,, \tag{3.28}$$

where $D^{res}_{8p,A}$ and $D^{res}_{8p,B}$ represents residual dipolar coupling for eight pulse sequence for groups A and B, respectively, and $D^{res}_{32p,A}$, $D^{res}_{32p,B}$ for thirty-two pulse sequence. Fitting errors were for both cases up to 2%. It has to be noted that PBM only hardly corresponds to the isolated two spin system so using the initial part of the build-up curve for fitting an error of about 10% ([Gra97a]) in real experiment is introduced. In addition group labeled as A in Figure 3.18 carries an information about overall residual dipolar coupling arising from $CH = CH$ and $CH - CH_2$ groups and group B from $CH - CH_2$ and CH_2 (intragroup) groups as can be seen from 2D DQ experiment (see Figure 3.10b). Hence, intergroup and intragroup couplings can not be distinguished from 1D DQ experiment. In spite of that neglecting chemical shift anisotropy comparison with two-dimensional DQ MAS experiment can be made where C7 pulse sequence was used (see section 3.3.1). Simple quadratic dependence of the dipolar coupling strength to the integrated intensity can be used (see equation 3.27) and assuming results (3.21) the ratio between residual

couplings from the group A and the group B can be calculated as[12]

$$(D_A^{res}) : (D_B^{res}) = 1.0 \,:\, 0.61\,. \tag{3.29}$$

Assuming an experimental error of around 10% for estimating of each residual coupling constant from results (3.21) the overall standard deviation error for estimating the ratio (3.29) can be up to 14% for each group, respectively. In spite of this relatively big error we find a good agreement with the results from thirty-two pulse sequence as well as from eight pulse sequence (ratios (3.28)).

3.5.2 Spin counting in polybutadiene rubber

Recently thirty-two pulse sequence proposed by Antzukin and Tycko has been used for exiting higher order coherences in singly-^{13}C-labeled organic solids (see section 2.4.1.3 and [Ant99]). In this section demonstration of excitation and detection of higher order coherences among ^1H nuclei in elastomers using this pulse sequence will be presented. Higher order MQ NMR spectroscopy has not been previously reported on elastomers. In strongly dipole-dipole coupled spin-½ systems in solids high-order MQ coherences were demonstrated over 16 years ago by Yen and Pines ([Yen83] and Figure 2.13) with the help of eight pulse sequence (see section 2.4.1.2 and Figure 2.13). In elastomers well above the glass temperature fast molecular motion reduce the dipolar coupling to few kHz. We found eight pulse sequence to be not enough effective to excite higher order coherences in high crosslinked polybutadiene rubber (PBR) presented in Figure 3.17c,d. Nevertheless thirty-two pulse sequence was more effective.

Up to the 6-th order of coherences were clearly visible in the proton spectrum of PBR with thirty-two pulse sequence. The experimental results are shown in Figure 3.19. MQ coherences are modulated by $\cos(p\,\Delta\phi \cdot m)$ function similar like in spin counting MQ experiment under MAS (see section 3.4). Hence, performing Fourier transformation with respect to m which represents second dimension, give rise to a series of δ-functions corresponding to the MQ coherence order p. Different orders of coherence are separated by $\Delta\phi = \frac{\pi}{p_{max}}$, where $p_{max} = 16$ to observe up to the 16-th order of coherent transitions. Single quantum (SQ) dimension (see Figure 3.19a) corresponds to the Fourier transformed signal which evolves in the direct ω_2 dimension during detection period (see Figure 2.14). In Figure 3.19b traces representing different groups CH and CH_2 are shown, respectively.

[12] Complementary normalization to the D_A^{res} was used.

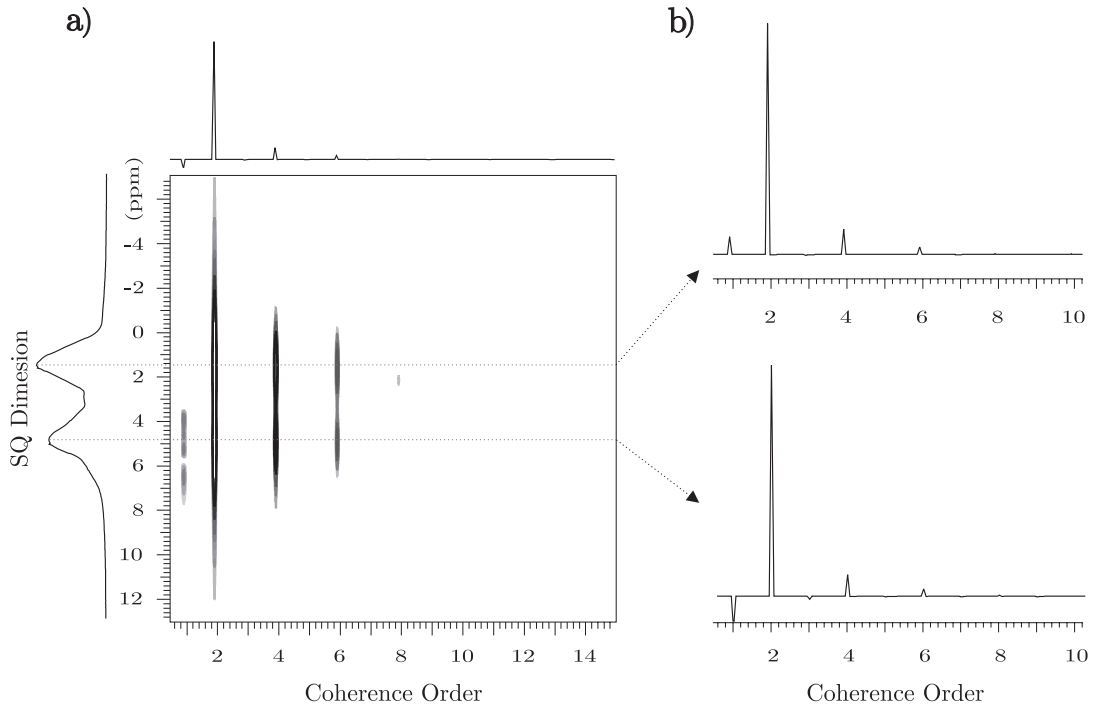

Figure 3.19: ^1H *spin counting MQ experiment for PBR (see page 91). MQ coherences were excited with thirty-two pulse sequence with excitation and reconversion time* $\tau = 8$ *ms. At the top and at the side of the figure* a) *projections of MQ coherences and single quantum (SQ) spectrum* (ω_2 *dimension) are shown, respectively (More details about SQ dimension see Figure 3.17c,d). Figure* b) *represents the traces corresponding to the different functional groups as it is indicated. To separate different orders of coherences* $\Delta\phi$ *was chosen* $11.25°$ *to resolve up to the 16-th order* ($p_{max} = 16$) *of coherence (more details see section 2.4.4). Only 32 phase increments were recorded corresponding to the full* 2π *cycle. The cycle time* τ_c *was 2 ms* ($t_p = 3.2$ μs, $\Delta = 163.4$ μs *and* $\Delta' = 330$ μs). *A delay of* $\tau_0 = 1$ *ms was included after reconversion period to allow unwanted transients to decay.*

Pulse imperfections and higher order correction terms in Magnus expansion (see equations (1.55) and (1.56)) leads to the odd-order signals in Figure 3.19b for both groups.

It has to be noted that it was quite difficult to observe higher order coherences in PBR. Most probably it is due to the fast relaxation of the spin system during excitation period. Relatively low dipole-dipole coupling strength caused by fast molecular motion force to choose long excitation/reconversion times τ to excite higher order coherences which interfere with relaxation of the spin system during this time τ. Solution of this problem might be to choose even high crosslinked samples or to decrease the temperature. It has to be stressed that decreasing the temperature leads to lowering the molecular

motion which increase the line-width, so static MQ spin counting experiment might by not able to resolve different functional groups. To overcome this difficulty high resolution MAS pulse sequences like C7 or POST C7 can be used in spin counting experiment (see section 3.4) to excite higher order coherences.